Uncovering the representational geometry of durations

Camille Grasso[1], Ladislas Nalborczyk[2], and Virginie van Wassenhove[3]

[1]Univ. Grenoble Alpes, Univ. Savoie Mont Blanc, CNRS, LPNC, 38000 Grenoble, France

[2]Aix Marseille Univ, CNRS, LPL, Aix-en-Provence, France

[3]CEA, DRF/Joliot, Neurospin; INSERM, Cognitive Neuroimaging Unit; Université Paris-Saclay, 91191 Gif-sur-Yvette, France

Author Note

Correspondence concerning this article should be addressed to Camille Grasso. E-mail: grassocamille@gmail.com.

Abstract

Is there a geometry of time in the human mind? A canonical measure of time in psychology is duration, a time interval quantifiable as a magnitude. Durations have been proposed to be arranged along a mental timeline: a unidimensional, linear, and spatialised representation of time. Here, we asked whether such a mental timeline is sufficient to account for the experience of duration. To address this, we tested the same participants in two experiments: a behavioural similarity judgment task, in which participants rated the similarity of duration pairs, and an electroencephalography (EEG) experiment in which they detected oddball durations in a sequence. Behavioural and EEG data were used to construct representational dissimilarity matrices, whose geometry was compared against theoretical models of duration organisation. Our results reveal that most variance in behavioural similarity judgements is explained by three latent dimensions, interpretable as: magnitude (monotonic ordering of durations), contextual encoding (distance to the geometric mean of the duration set), and a periodic component. These three dimensions are jointly consistent with a latent generalised helical model, which provided excellent fit to the behavioural data. Individual helical model parameters further correlated with endogenous neural oscillations measured during rest, suggesting that an individual's duration space is partially constrained by intrinsic dynamics. The neural geometry was also found to be dynamic, unfolding in two successive stages: a strong logarithmic encoding of durations peaking around 150 ms after duration offset, followed by a spring-like geometry starting around 300 ms after offset. Together, these findings describe multidimensional psychological and neural geometries of duration space, and characterise their relationship.

Keywords: time perception, interval timing, duration processing, conceptual spaces, representational geometry

Introduction

All experiences unfold in time, making time a fundamental dimension of perception, action, and cognition. Characterising how the brain represents time is therefore a central challenge for cognitive neuroscience (e.g., Buonomano et al., 2023; Buzsáki, 2026; Kwok et al., 2025; Ma et al., 2024; Paton & Buonomano, 2018; Tsao et al., 2022). However, the representational principles governing the coding of time intervals across scales, from subsecond to suprasecond durations, remain poorly understood. What, then, is the structure of the internal space in which durations are represented?

Several influential frameworks have proposed that time is spatialised along a mental timeline (e.g., Bonato et al., 2012; Vallesi et al., 2008; Vicario et al., 2008). In many of these accounts, durations are conceived as magnitudes organised along a single internal dimension, with shorter and longer intervals ordered monotonically along a time axis (e.g., Bender & Beller, 2014; Bueti & Walsh, 2009; Walsh, 2003). This view captures important features of duration judgement but leaves unresolved the structure of duration representations themselves. More specifically, whether the psychological and neural representations of duration can be reduced to a single latent axis, or whether they are better characterised as a higher-dimensional geometry remains to be addressed.

A constructive way to approach this question is to adopt a relational approach to the representation of durations: instead of asking how a given duration is represented in isolation, we can asks how durations are positioned relative to one another in terms of perceived similarity. This idea builds on the foundational insight that, even when direct correspondences between internal representations and external referents are difficult to establish, lawful structure may still be recovered from the relations among representations (Shepard & Chipman, 1970). Pairwise similarity judgements offer an empirical window onto the structure of mental representations, while multidimensional scaling (MDS) provides a formal tool for recovering the latent geometry that organises those judgements (e.g., Kruskal, 1964; Kruskal & Wish, 1978; Shepard, 1980, 1987; Shepard et al., 1975; Sievers et al., 2021; Torgerson, 1977).

This relational logic has been extended to neural data through representational similarity analysis (RSA, Kriegeskorte & Kievit, 2013). In this framework, activity patterns elicited by each condition are treated as points in a high-dimensional space, and the pairwise dissimilarities between these patterns are summarised in a representational dissimilarity

matrix (RDM). Crucially, because RDMs are defined over conditions rather than over specific sensors, neurons, or voxels, they provide a common representational format that can be compared across behavioural data, neural recordings, computational models, individuals, and species (Kriegeskorte & Kievit, 2013). RSA and related approaches have been applied across a broad range of cognitive domains, including perception (e.g., Fournel et al. 2016; Kriegeskorte et al. 2008), abstraction (e.g., Chung & Abbott, 2021; Nieh et al., 2021), decision-making (e.g., Van Baar et al., 2019), and social cognition (e.g., Tamir et al., 2016; Thornton & Mitchell, 2018).

A key advantage of this framework is that the geometry of representational spaces can reveal the computational principles that structure a given cognitive domain. For instance, in colour perception, pairwise similarity judgements have long been known to recover an internal organisation closely related to the perceptual colour wheel (e.g., Shepard & Cooper, 1992). Recent work has shown that the geometry derived from similarity judgements is sufficiently sensitive to capture subtle differences in colour experience across the visual field (e.g., Zeleznikow-Johnston et al., 2023), between groups of colour-neurotypical and colour-atypical observers, and between humans and large language models (e.g., Kawakita et al., 2024, 2025). At the neural level, multivariate analyses of magnetoencephalography (MEG) responses have revealed a dynamic colour geometry predictive of universal colour-naming patterns, illustrating how representational geometry can bridge neural activity and perceptual experience (Rosenthal et al., 2021). Similar principles have also been identified in audition, where pitch perception is organised along a helical structure (e.g., Shepard, 1982; Ueda & Ohgushi, 1987). In this helical structure, tones separated by an octave occupy analogous positions across successive turns. This geometry captures both monotonic variations in pitch height and periodic variations in chroma (e.g., Chang et al., 2025; Marjieh et al., 2023, 2024; Shepard, 1982; Ueda & Ohgushi, 1987). These examples show that similarity structure can reveal representational organisations that are not reducible to a single linear axis.

We therefore applied this approach to time perception and asked how many latent dimensions organise the human psychological space of durations. By ‘dimension’, we refer to a latent organising axis within a psychological space, here termed the duration space. In this view, duration space is a representational geometry in which durations vary systematically, such that pairwise similarities between them can be approximated by distances in a

low-dimensional space. These dimensions are not assumed to map one-to-one onto single neural variables (i.e., they do not imply isomorphism; Gallistel, 1990; van Wassenhove, 2009); rather, they provide a formal bridge between behavioural and neural representational structures.

We tackled this question by combining behavioural similarity judgements with electroencephalography (EEG) recordings within a common representational framework. In a first experimental session, participants rated the perceived similarity of all possible pairs of auditory durations. Behavioural data served the estimation of the geometry of duration representations in participants' psychological space. In a second session, EEG was recorded while the same durations were presented to the same participants. RDMs were derived from EEG recordings and the multivariate similarity structure of evoked responses. Behavioural and neural RDMs were then compared with the predictions of theoretical models of duration organisation.

We hypothesised that the psychological space of durations would not be adequately captured by a single dimension, but would instead require at least two latent dimensions (Bailly et al., 2011). Our findings went beyond this prediction. They suggest that at least three organising principles are needed to account for the relational structure of duration space. The first is a magnitude dimension, reflecting the monotonic ordering of durations, potentially in a compressive form consistent with scalar timing. The second is a contextual dimension, capturing the encoding of durations with respect to the centre of the experienced distribution. The third, more exploratory, is a periodic dimension, which may reflect similarity relations induced by endogenous neural rhythms. At the neural level, geometry was found to be dynamic, unfolding in two successive stages: a strong logarithmic encoding of durations peaking around 150 ms after duration offset, followed by a spring-like geometry, converging with the behavioural structure, starting around 300 ms after duration offset.

Methods

Participants

Thirty-three healthy adults (mean age: 26.97 years; 19 female) were recruited through university mailing lists and the RISC's participant pool (https://www.risc.cnrs.fr/). All participants reported normal or corrected-to-normal vision, and no history of neurological or psychiatric disorders. All were naive as to the purpose of the study.

Ethics information

The study was approved by the Ethics Committee for Research (CER) of Paris-Saclay University (CER-Paris-Saclay-2023-089). Written informed consents were obtained from all participants in accordance with the guidelines of the Ethics Committee. Participants were compensated 20 € for the first behavioural session and 90 € for the second EEG session.

Similarity judgment task (behaviour)

Both the similarity judgment and oddball detection tasks were implemented in PsychoPy v2021.2.3 (Peirce et al., 2019). The experiment consisted of two separate sessions conducted in a quiet EEG-dedicated room at NeuroSpin (CEA/DRF, Gif-sur-Yvette, France), where participants remained seated comfortably in an armchair throughout the procedure.

To investigate the structure of duration representations, participants performed a similarity judgment task involving pairs of auditory (440 Hz pure tone) durations (Figure 1). Each duration was drawn from a fixed set of ten durations ranging from 400 ms to 2200 ms in 200 ms steps (i.e., covering sub- to supra-second range). On each trial, pairs of durations were presented with an inter-stimulus interval of 700 ±10% ms. Their order was counterbalanced. To ensure that similarity judgments were based on duration rather than accumulated perceptual intensity, the loudness of each stimuli was randomly varied by ±5 dB around a base level of 70 dB, thereby reducing the potential influence of energy-based cues associated with longer durations (Dai & Micheyl, 2010). All 45 possible pairs of durations were presented in both orders, yielding a total of 90 pairs of durations per participant. Participants judged the perceived similarity of the pair on each trial (1 = 'most dissimilar', 7 = 'most similar') using the computer mouse. A 1000 ms inter-trial interval followed each response before the onset of the next trial.

Before the task, participants received standardised instructions both orally and in written form on screen, followed by a short practice phase consisting of 20 trials (duration pairs) composed of the most representative durations of the stimulus set (i.e., the smallest, the largest, and three intermediate durations), allowing them to familiarise themselves with the procedure and the rating scale. The task was divided into four blocks, each containing all 90 duration pairs presented in a randomised order. Each block lasted approximately 10 minutes, for a total session duration of approximately 50 minutes. Short breaks were offered between blocks. Participants could also take self-paced pauses within a block by withholding their

response before initiating the next trial. Across the four blocks, each participant completed 360 trials, yielding a complete matrix of pairwise similarity ratings among the ten durations. Participants were explicitly instructed to refrain from counting or tapping to estimate durations (Rattat & Droit-Volet, 2012).

Oddball duration task (EEG)

Participants returned to the lab for the second session, approximately one week after the behavioural session. During this EEG session, participants performed a duration oddball detection task, designed to capture neural responses underlying the encoding of durations in the absence of explicit motor demands (i.e., button presses). Participants listened to a continuous stream of durations (as in the behavioural task, 440 Hz pure tones). Standard durations in the stream were randomly selected from the set of ten durations used in the similarity judgment task (400 ms to 2200 ms in 200 ms steps; 80% of trials). The deviant durations were 70 ms and 3400 ms (20% of trials) and were selected based on pilot data (N = 5) to ensure reliable perceptual discrimination from the standards. Participants were instructed to monitor the duration of each tone and detect oddballs (deviant durations) by pressing the space bar as quickly and as accurately as possible. The shorter- and longer-than-standard oddballs were included to ensure that participants monitored the full temporal extent of each stimulus. As in the similarity judgment task, stimulus intensity was randomly jittered by ±5 dB around a baseline of 70 dB to minimise reliance on cumulative intensity as a cue, ensuring that participants focused on temporal duration per se. The inter-stimulus interval was fixed at 700 ms, jittered by ±10% to prevent rhythmic entrainment (see Figure 1 for a schematic representation of the trial sequence).

A trial-level feedback system was implemented to maintain task engagement. Correct detections (hits) were signalled by a green fixation cross, whereas missed oddballs or responses to standard stimuli (false alarms) triggered a red fixation cross. Only standard trials without response were retained for subsequent analyses.

EEG data acquisition

EEG data were recorded using a 64-channel Waveguard cap (ANT Neuro, Enschede, Netherlands) mounted on the participant's scalp. CPz served as the online reference electrode. EEG data were acquired using an eego mylab amplifier system at a sampling rate of 1000 Hz, a 131 Hz low-pass filter applied online and no high-pass filter. Impedances were kept below 20

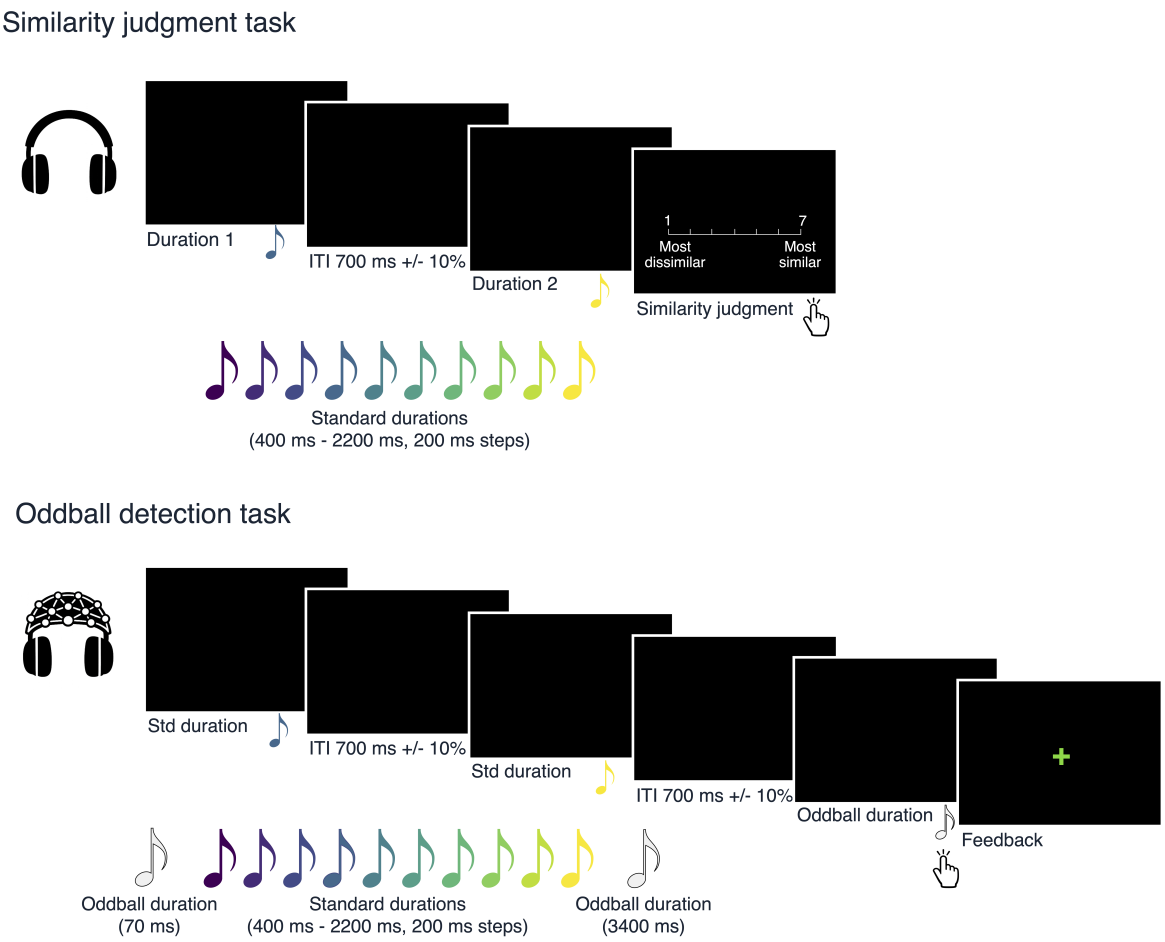

Figure 1. ***Overview of the experimental protocol. Top row: Similarity judgment task.*** *On each trial, participants heard two tones in succession and judged how similar their duration felt on a 7-point Likert scale, from 'most dissimilar' to 'most similar'.* ***Bottom row: Oddball detection task.*** *Participants listened to the same durations as in the behavioural experiment, but this time they were presented as a continuous stream with varying ITIs. Participants were tasked to detect rare duration oddballs, which were shorter or longer than all other standard durations. Responses were made by pressing the space bar, and visual feedback indicated correct detections and errors.*

kΩ at all times. Vertical eye movements were monitored via electrooculography (EOG), with one electrode placed above the left eye.

EEG data preprocessing

Continuous EEG data were preprocessed using custom Python scripts and `MNE-python` software (Gramfort, 2013). Noisy or malfunctioning (e.g., flat) electrodes were identified by visual inspection, and participant-specific bad channels were annotated. Time periods containing muscular artifacts were also annotated. Ocular and other stereotyped artifacts were corrected using independent component analysis (ICA) computed separately for each block. ICA was fit on a temporally filtered copy of the data (high-pass above 1 Hz) to improve decomposition stability, while the resulting unmixing was applied to the corresponding

unfiltered continuous signal. Components reflecting eye blinks and saccades were identified using EOG-channel correlations and marked for rejection, after which ICA was applied to obtain cleaned continuous data. The cleaned signal was then re-referenced to the common average reference, and previously marked bad channels were interpolated using spherical splines. Mastoid electrodes (M1 and M2) were excluded from all analyses, as they consistently exhibited high noise levels across participants and do not capture cortical activity (Cohen, 2014). The cleaned continuous data were band-pass filtered (0.1-40 Hz) and segmented into epochs time-locked to duration offset. At epoching, time segments previously annotated as artifacts were automatically excluded. Finally, we removed trials containing participants' responses and trials corresponding to 'odd' durations, before applying a baseline correction using a [-100 ms, 0] interval relative to duration offset.

Data analysis

Behavioural data

Preprocessing similarity ratings. We summarised the similarity judgments of each participant in a representational dissimilarity matrix (RDM) according to the following procedure. Each similarity rating, initially provided on a 7-point Likert scale (1 = the most dissimilar, 7 = the most similar), was rescaled to the [0, 1] interval and converted to a dissimilarity score (i.e., 1 – rescaled similarity). For each participant, dissimilarity scores were then averaged across all repetitions of a given duration pair, yielding a 10×10 RDM in which each entry reflects the perceived dissimilarity between two durations.

Multidimensional scaling. To visualise the global structure of the duration space, we applied non-metric multidimensional scaling (MDS, Kruskal, 1964) to each participant's RDM. This technique embeds high-dimensional dissimilarity data into a low-dimensional geometric space while preserving the rank order of pairwise distances. To determine the dimensionality of the MDS solution, we computed stress values for embeddings spanning one to five dimensions. Stress quantifies the mismatch between the dissimilarities in the original RDM and the distances between points in the reduced-dimensional space, thereby providing a criterion for selecting the number of dimensions that best captures the structure of the data (Kruskal, 1964; Kruskal & Wish, 1978).

Theoretical models. We next sought to assess how well the structure of the duration space, captured in the empirical RDM, could be explained by different theoretical

accounts of duration representation. To this end, we constructed a set of theoretical RDMs, each embodying a specific hypothesis about the geometry of duration encoding (Table 1).

To assess how well each model accounted for participants' empirical similarity judgments, we computed the Spearman rank-order correlation between the empirical RDM and each theoretical RDM. Before computing the correlation, we extracted the upper triangular part of each matrix (excluding the diagonal) to avoid redundancy and trivial self-comparisons. These elements were then flattened into 1D vectors of length 45. The resulting vectors captured the full set of unique pairwise dissimilarities in each RDM. The Spearman correlation coefficient thus provided a measure of model-data fit, robust to non-linear scaling. This approach allowed us to compare the internal structure predicted by each theoretical model to the structure derived from participants' subjective similarity judgments.

Model comparison. Because theoretical RDMs vary in flexibility (0, 1, or 2 free parameters), we used a leave-one-duration-out cross-validation procedure to obtain an unbiased estimate of their predictive accuracy and prevent overfitting. For each left-out duration d_k (10 folds in total):

1. Training set: We removed duration d_k and its associated row and column from the empirical RDM, yielding a 9×9 sub-RDM. Parametrised models (i.e., Helix and Power) were fitted only to this sub-RDM, by minimising the negative Spearman correlation between the flattened upper-triangular part of the empirical and model-predicted RDMs.

2. Testing set: Using the fitted parameters $\hat{\theta}^{(k)}$, each model generated a full 10×10 predicted RDM. The model's *out-of-sample prediction error* was computed exclusively on the left-out row and column (i.e., all dissimilarities involving d_k).

3. Fold score: We quantified predictive accuracy for fold k as the Spearman correlation between the empirical dissimilarities $\mathcal{E}(d_k, d_j)$ and model-predicted dissimilarities $\mathcal{M}(d_k, d_j \mid \hat{\theta}^{(k)})$ for all $j \neq k$. This produced 10 fold-wise correlation values per model:

$$\rho_k = \mathrm{cor}\big(\mathcal{E}_{k,-k}; \mathcal{M}_{k,-k}(\hat{\theta}^{(k)})\big),$$

which we then averaged to yield the average cross-validated model score:

Table 1

Summary of theoretical models and their dissimilarity functions.

Model	Description	Dissimilarity function
Linear	The Linear model serves as the simplest metric baseline: it assumes that subjective dissimilarity grows in direct proportion to the absolute physical difference between two durations, that is: psychological distance preserves objective elapsed-time differences without compression or categorical warping.	$\mathcal{M}_{\text{linear}}(d_i, d_j) = \lvert d_i - d_j \rvert$
Logarithmic	The Logarithmic model tests the idea that duration may be represented on a compressed internal scale, consistent with the Weber-Fechner's law and with broader accounts in which perceptual systems code magnitudes approximately logarithmically or according to relative rather than absolute differences (e.g., Gallistel & Gibbon, 2000; Gibbon, 1977).	$\mathcal{M}_{\log}(d_i, d_j) = \lvert \log d_i - \log d_j \rvert$
Binary	The Binary model operationalises the possibility that listeners do not preserve fine-grained metric structure across the full range, but instead partition durations into coarse categories such as 'short' versus 'long' relative to the mean of the duration set (1300 ms).	$\mathcal{M}_{\text{binary}}(d_i, d_j) \in \{0, 1\}$
Random	The Random model is not meant as a psychological theory of duration representation, but as a null-structure control: it provides a lower-bound benchmark against which theory-driven model fits can be interpreted.	$\mathcal{M}_{\text{random}}(d_i, d_j) \sim \text{Uniform}(0, 1)$
Free-parameter models		
Power	The Power model is motivated by Stevens' psychophysical law, which proposes that subjective magnitude is a power function of physical magnitude (e.g., Stevens, 1957). Applied to time, it captures a flexible family of monotonic non-linear transformations, allowing subjective duration to expand or compress as a function of the exponent parameter α. This makes it a principled alternative to both strictly linear and strictly logarithmic scaling.	$\mathcal{M}_{\text{power}}(d_i, d_j \mid \alpha) = \lvert d_i^{\alpha} - d_j^{\alpha} \rvert$
Helix	The Helix model is an embedding-based model in which each duration is mapped onto a point in a three-dimensional latent space lying on a parametrised generalised helical trajectory (see Appendix A). Dissimilarities correspond to Euclidean distances between embedded points. This model tests whether duration similarity may reflect a representational space with both a monotonic dimension and an additional cyclic component (Bailly et al., 2011).	$\mathcal{M}_{\text{helix}}(d_i, d_j \mid \Theta) = \lVert \mathbf{x}(d_i; \Theta) - \mathbf{x}(d_j; \Theta) \rVert_2$

Note. Free parameters of the Power and Helix models were optimised via an iterative optimisation process to find the configuration that maximised the Spearman correlation between the model-based RDM and the empirical RDM for each participant.

$$\text{CV-score} = \frac{1}{10}\sum_{k=1}^{10}\rho_k.$$

We stored the fitted parameters from each fold to assess parameter stability across folds. Models were compared on their median cross-validated correlation, which provides an unbiased estimate of how well each model predicts dissimilarities for durations it was *not* trained on. Because the metric reflects genuine out-of-sample performance, more flexible models only outperform simpler ones if their additional parameters capture structure that generalises across durations, rather than overfitting idiosyncrasies of the empirical RDM. After model comparison, we also fitted each parametrised model to the full empirical RDM (using the same correlation-based objective) to obtain a single set of interpretable parameters for visualisation and analysis. These 'full-data' fits were not used for model comparison.

Group-level statistical inference. To assess the results of the model comparison procedure while accounting for the skewed distribution of CV scores, we fitted a Bayesian multilevel generalised linear model using the `brms R` package (Bürkner, 2017, 2018; Nalborczyk et al., 2019). More precisely, we fitted a skew-normal multilevel model that estimates the average CV score per theoretical model, both at the participant and group levels, while allowing the dispersion and skewness of CV scores to vary per theoretical model. This model was fitted using weakly informative priors (see the supplementary materials for code details). Eight Markov Chain Monte-Carlo (MCMC) were run for each model to approximate the posterior distribution, including each 5000 iterations and a warmup of 1000 iterations. Posterior convergence was assessed examining trace plots as well as the Gelman-Rubin statistic. Constant effect estimates were summarised via their posterior mean and 95% credible interval (CrI), where a credible interval can be considered as the Bayesian analogue of a classical confidence interval. When applicable, we also report Bayes factors (BFs), computed using the Savage–Dickey method, which consists in taking the ratio of the posterior density at the point of interest divided by the prior density at that point. These BFs can be interpreted as an updating factor, from prior knowledge (what we knew before seeing the data) to posterior knowledge (what we know after seeing the data).

EEG data

Event-related potentials. In a first step, we aimed at identifying clusters of sensors that responded to (or 'encoded') durations. To this end, we fitted a regression to predict EEG activity at duration offset for each participant, sensor, and timestep, using durations recoded using their rank (in ascending order) as a predictor. We used ranks not to impose a linear constraint on the identification of the channels, as this would bias the subsequent RSA in favour of the linear model. This analysis resulted in a slope estimate representing the monotonic effect of duration for each participant, sensor, and timestep. We then concatenated these 2D matrices into a 3D tensor of shape participants, channels, timesteps, and used a cluster-based permutation test with threshold-free cluster enhancement (TFCE; Smith & Nichols, 2009) to identify clusters of sensors and timesteps with slopes significantly different from 0.

Time-frequency analysis. To analyse induced oscillatory power across frequency bands at duration offset, we computed time-frequency representations (of the EEG temporal signals without baseline correction) using Morlet wavelets. These analyses were performed over a range spanning -2000 to 2000 ms relative to duration offset. Time-frequency decomposition was conducted across frequencies from 4 to 40 Hz in 1-Hz steps, encompassing canonical frequency bands from theta to low gamma. Frequencies below 4 Hz were excluded due to the limited epoch length. The number of wavelet cycles was set to half the center frequency, providing an optimal trade-off between temporal and spectral resolution. Time-frequency representations were then cropped to provide the final analysis window, spanning from -100 ms to 600 ms relative to duration offset. These power estimates were then normalised by taking the logarithm of the ratio of the period of interest over a [-100 ms, 0] baseline period (relative to offset). To isolate the induced oscillatory activity, we subtracted the evoked response (i.e., the across-trial per-condition average) from each epoch (David et al., 2006). We then averaged power in the theta (4–7 Hz), alpha (7–13 Hz), beta (13–30 Hz), and low-gamma (30–40 Hz) bands.

Representational similarity analysis. To characterise the relationship between similarity judgments, theoretical models, and EEG representations of duration in the oddball task, we performed a time-resolved representational similarity analysis (RSA). This analysis relied on the same set of theoretical RDMs used for the behavioural analyses, together with

participant-level RDMs derived from EEG data. In addition to the theoretical models previously described (Table 1), we designed a novel RDM capturing similarities in the difference between each duration and the closest odd duration (i.e., 70 ms or 3400 ms), thus capturing a unique task-relevant feature.

EEG RDMs were computed within the $[-100, 600$ ms$]$ interval relative to duration offset using cross-validated representational dissimilarities, as implemented in the `mne-rsa` toolbox (Van Vliet et al., 2025). For each time point, we estimated a 10x10 pairwise dissimilarity matrix using a cross-validated squared Euclidean distance (i.e., a cross-validated dissimilarity metric derived from squared Euclidean distances computed on multichannel EEG patterns). Specifically, trial-level EEG patterns were partitioned into folds and dissimilarities were computed in a cross-validated manner across folds, yielding a time-resolved series of condition-by-condition RDMs for each participant. These time-resolved EEG RDMs were then compared to the theoretical RDMs using Spearman correlations.

To further disentangle the unique contribution of each theoretical model in explaining the EEG variance, we then applied commonality analysis (e.g., Cichy & Oliva, 2020; Hebart et al., 2018; Seibold & McPhee, 1979) to quantify the relationship between behavioural and EEG RDMs while accounting for multiple theoretical RDMs. This variance-partitioning approach enables the decomposition of shared variance into components that are common to behaviour, EEG, and the theoretical models, while statistically controlling for variance uniquely attributable to the remaining models.

This analysis yielded, for each participant, a time-resolved estimate of the unique (partial) correlation between EEG RDMs and each theoretical RDM. To assess whether these time courses differed across theoretical models at the group level, we fitted a series of Bayesian generalised additive multilevel models using the `brms` R package (Bürkner, 2017, 2018; Nalborczyk et al., 2019). This modelling framework provides posterior odds for non-null effects at each time point while explicitly accounting for temporal dependencies as well as within- and between-participant variability. Importantly, this approach has been shown to yield more reliable and temporally precise estimates of the onset and offset of time-resolved M/EEG effects than cluster-based permutation tests (Nalborczyk & Bürkner, 2025).

Linking duration representations to neural dynamics. To elucidate the neural correlates of the representational geometry revealed by the behavioural data, we next sought

to relate parameters of the theoretical models fitted to the behavioural RDMs to EEG features measured both i) during task performance (hereafter referred to as task-related EEG features) and ii) during out-of-task periods (hereafter referred to as endogenous EEG features).

As task-related EEG feature, we used the amplitude and the latency of the offset P2, computed over six clustered frontocentral electrodes: FC1, FCz, FC2, C1, Cz, and C2 (Baykan et al., 2023; Damsma et al., 2021; Kononowicz & Van Rijn, 2014; Ng et al., 2011; Ofir & Landau, 2022). We additionally analysed the average theta, alpha, beta, and gamma power in the $[0 - 200$ ms] interval following duration offset. As endogenous EEG features, we used the intercept and exponent of the aperiodic (1/f) component, as well as the peak frequency and bandwidth of the alpha and beta bands (Donoghue et al., 2020), estimated during a movement-free 15-to-45 s period (exact duration varied across participants) of between-block resting state.

Results

Behavioural data

Psychological duration space

We first asked whether participants' similarity judgements revealed a coherent representational structure for duration, and if so, what its broad organisation looked like at the group level. Figure 2A shows the average behavioural RDM at the group-level. As expected, the matrix displays a clear diagonal structure: pairs of similar objective durations were judged as more similar. The matrix also reveals an apparent decrease in discriminability with increasing duration: dissimilarities in the upper-right corner (longer durations) are generally lower than those in the lower-left corner (shorter durations). Interestingly, RDMs at the participant-level exhibited substantial inter-individual variability in both structure and noise (Appendix B), such that some fine-grained patterns were attenuated or lost when averaging across participants. This underscores the importance of analysing representational structure at the level of individual participants.

The asymmetry matrix, computed as $A = D - D^T$, reveals a striking and systematic order effect (Figure 2B). For duration pairs shorter than the average duration (1300 ms), the first-presented duration tended to be judged as longer than when the same duration appeared second. For pairs longer than the average of the tested distribution, the pattern reversed. Because these asymmetries reflect task-induced, order-dependent biases, rather than intrinsic

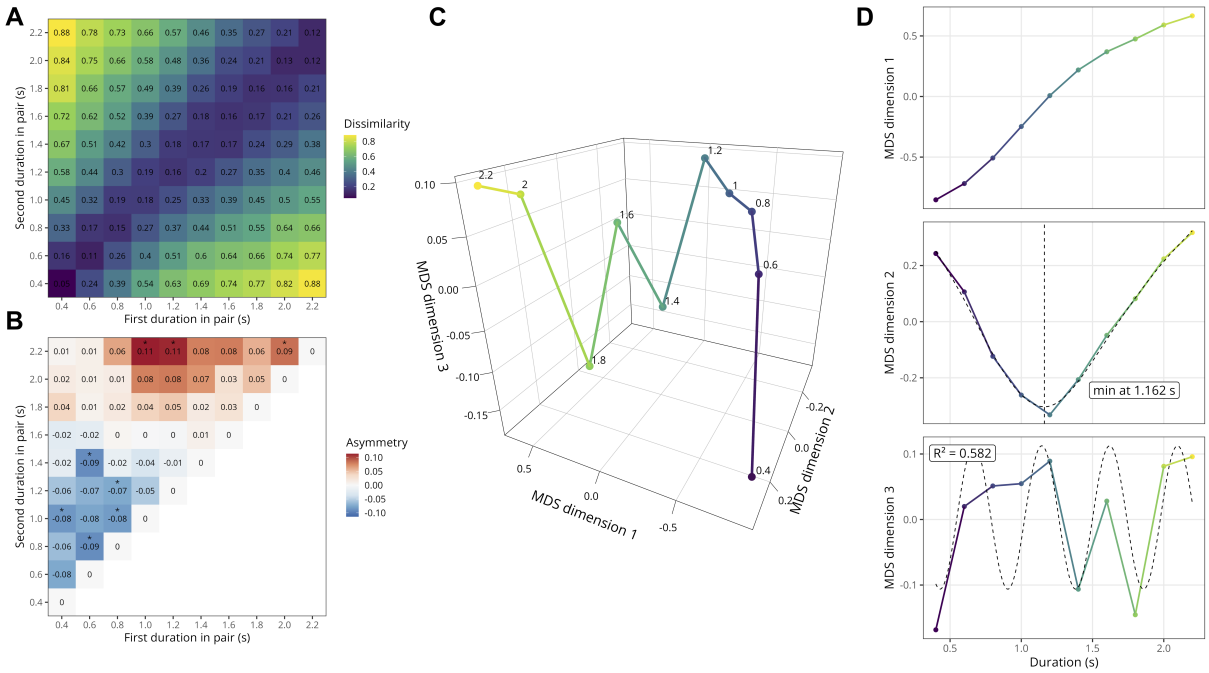

Figure 2. ***Geometry of the duration space (behaviour).*** ***A.*** *Empirical dissimilarity matrix derived from duration similarity judgements averaged at the group-level. Each cell shows the mean dissimilarity assigned to a pair of durations (s). Lower values (blue) indicate that two durations were perceived as more similar, whereas higher values (yellow) indicate that they were perceived as more dissimilar. The matrix shows a clear diagonal organisation, with dissimilarity increasing as the difference between durations grows.* ***B.*** *Group-level asymmetry matrix, computed as* $A = D - D^T$*. This panel highlights directional deviations from perfect symmetry in pairwise judgements. Red cells indicate pairs for which the dissimilarity was greater in one presentation order than in the reverse order (positive asymmetry), whereas blue cells indicate the opposite pattern (negative asymmetry). Values close to zero (white) indicate little or no order-dependent asymmetry. Stars indicate pairs of durations with statistically different order asymmetries (BF10s* > 3*).* ***C.*** *Three-dimensional MDS solution fitted to the average empirical dissimilarity matrix. Each point corresponds to one duration. Neighbouring points represent durations judged as more similar. The embedding reveals a structured trajectory across durations rather than a simple linear arrangement.* ***D.*** *Coordinates of the three MDS dimensions plotted as a function of objective duration. The first dimension varies monotonically with duration, suggesting that it captures the main ordinal progression from short to long intervals. The second dimension shows a U-shaped profile with a minimum around 1.16 s, indicating sensitivity to distance from a central tendency. The third dimension shows a periodic-like modulation across durations (which can be described by a sinusoidal function, represented by the dashed curve), consistent with an additional oscillatory or cyclic component in the representational geometry.*

properties of duration representation, all subsequent analyses focus on order-invariant structure. To this end, we symmetrised each participant's RDM prior to MDS and model comparison.

To uncover the geometry of the duration space at the group-level, we first aligned individual MDS solutions to a common coordinate frame using generalised Procrustes analysis (Gower, 1975). Then, we averaged the resulting 3D coordinates across individuals (Figure 2C). A comparison with INDSCAL; a hierarchical MDS procedure; yielded qualitatively similar embeddings. A scree plot analysis of stress values revealed an elbow at three dimensions, beyond which higher-dimensional solutions provided only marginal improvements. We therefore retained the 3D MDS solution for all subsequent analyses.

The resulting 3D embeddings reveal a clear non-linear organisation of subjective durations (Figure 2C), resembling a corkscrew or spring-like trajectory predominantly oriented along the objective-duration axis. This first dimension captures a monotonic ordering of durations by magnitude, scaling subjective duration with physical duration. The second dimension appears to encode the eccentricity of a duration relative to the geometric mean of the set of durations. The third dimension captures a periodic component, with clear peaks and valleys.

Figure 2D also shows the 1D projections of the 3D group-level MDS embeddings in relation to objective duration. This figure confirms that the first MDS dimension arranges durations in a monotonic fashion. The second MDS dimension arranges durations according to their 'distance' to a value (≈ 1.162 s) very close to the geometric mean of the durations set (≈ 1.151 s). The third MDS dimension arranges durations in a periodic pattern that was adequately described by a sinusoidal function (optimal period of ≈ 476 ms, $R^2 \approx 0.582$).

Model comparison

Given the large degree of inter-individual variability in behavioural similarity judgements (cf. Appendix B), we performed the subsequent analyses at the participant level. Figure 3A shows the results of the model comparison procedure for one exemplary participant. This figure shows that, overall, all theoretical RDMs provided a good fit to the empirical RDM (all Spearman's $\rho > 0.7$) with similar looking patterns.

Figure 3B presents the group-level RSA results, showing the distribution of raw optimised correlation values (top row) and cross-validated correlation values (bottom row) for each candidate model. Models are ordered vertically according to their performance, indexed by the median cross-validated correlation. Overall, two models consistently provide the best fit to the empirical RDMs: the Helix and Power models. Importantly, the bottom panel indicates that cross-validation preserves the relative ordering of models, suggesting that model ranking is not driven by overfitting. However, cross-validation attenuates the differences between models, notably reducing the performance gap between the optimised models (i.e., Helix and Power) and the non-optimised models (Linear and Log models).

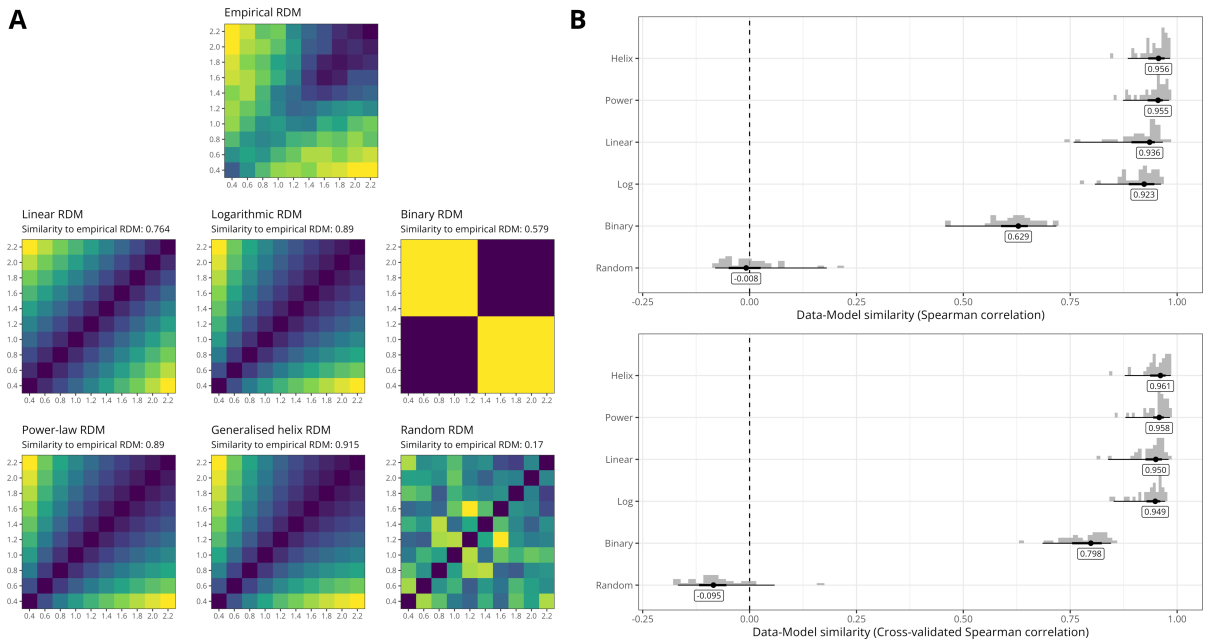

Figure 3. ***Behavioural RSA results. A.*** *RSA results for one exemplary participant. The top row shows the average symmetrised empirical RDM (i.e., subjective similarity ratings) whereas the second and third rows show the model RDMs along with their Spearman correlations to the empirical RDM.* ***B.*** *Group-level results of the model comparison. Top panel shows the raw (uncorrected) Spearman correlation for each model, whereas the bottom panel shows the cross-validated score. In both panels, models are vertically arranged by their median similarity to the empirical RDM. Densities show the distribution of similarities across participants. The dots and error bars show the median along with the 50 and and 95 % central quantiles of this distribution.*

EEG data

Event-related potentials

Having characterised the geometry of duration space at the psychological level, we next examined its neural geometry. We focused on activity time-locked to duration offset, as this marks the point at which the full temporal interval has become available to the system. This alignment is therefore the most direct for testing neural signatures of represented duration. All analyses reported below were performed on offset-locked data. Figure 4A shows the group-level scalp distribution of the t-values associated with the slope estimates from the rank linear regression, sampled over the 600 ms following stimulus offset. The effect was robust and temporally sustained across this post-offset window. Its topography showed negative t-values over fronto-central sensors (blue) and positive t-values over parieto-occipital sensors (red), revealing a clear anterior–posterior polarity.

Figure 4B shows the group-level average ERP time-locked to stimulus offset for each duration, averaged the fronto-central cluster of electrodes identified by the cluster-based permutation test (shaded areas indicate variability across participants). Shortly after offset, the evoked response diverges as a function of duration. A pronounced positive-going deflection

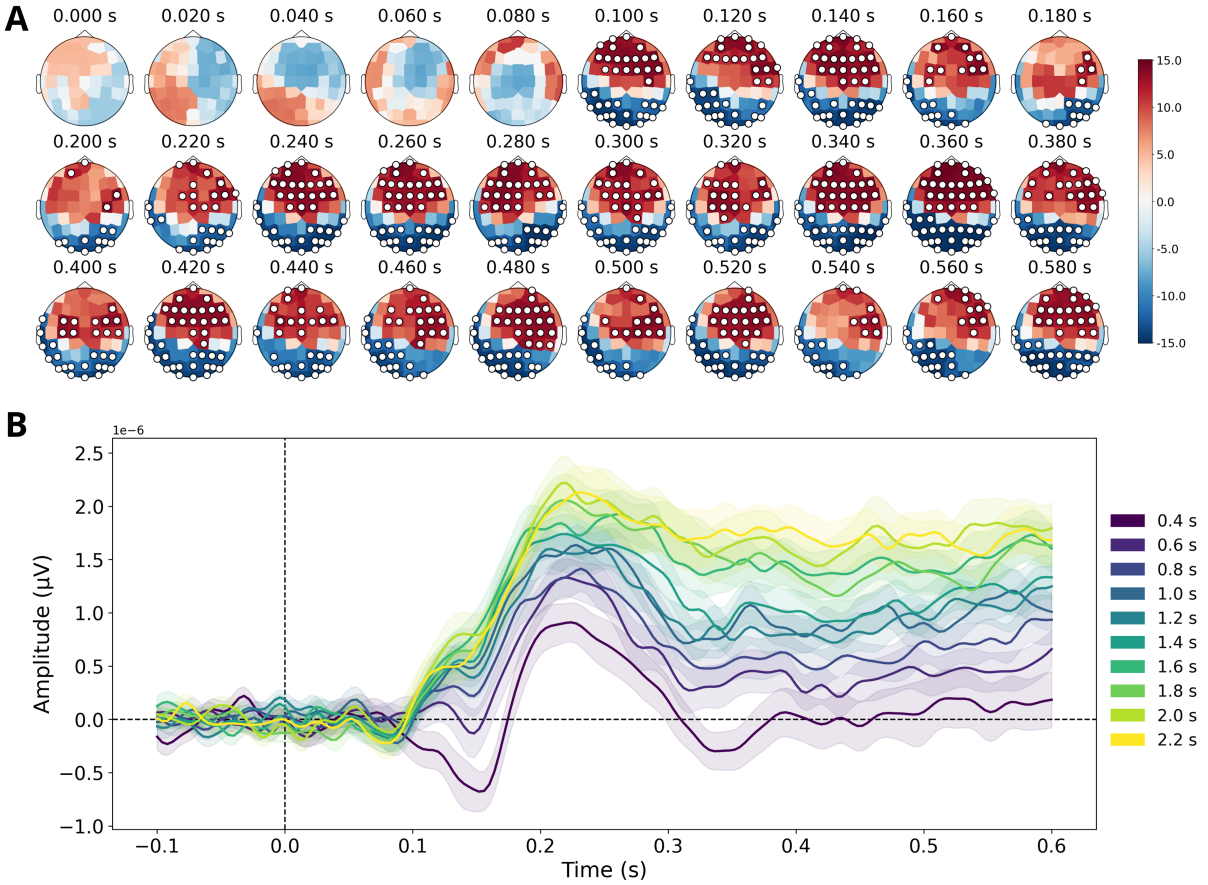

Figure 4. ***Event-related potentials at duration offset. A.*** *Group-level t-values of the slopes as estimated by the rank linear regression at duration offset. Spatio-temporal clusters (indicated by labelled sensors) were determined via spatio-temporal cluster-based permutation tests with TFCE and a significance threshold* $\alpha = .05$. ***B.*** *Group-level average ERP computed within the fronto-central cluster. Each coloured line represents the average EEG activity within this cluster for a given duration. The ribbon spans an interval of +/- 1 standard error of the mean.*

emerges around $\approx 120 - 150$ ms, peaks around $\approx 180 - 220$ ms, and is followed by a sustained positivity extending through ≈ 600 ms. Crucially, both the peak amplitude and the later sustained activity scale monotonically with duration: longer durations (green/yellow traces) show the largest positive amplitudes, whereas shorter durations (purple/blue traces) remain smaller and closer to baseline.

EEG representational structure through time

Having established the behavioural geometry of duration judgments, we next asked whether a comparable structure could be tracked in neural activity, and if so, when it emerges over time. To address this question, we examined the group-level average EEG RDMs across successive post-offset time windows, together with their associated 2D MDS embeddings (Figure 5). This analysis revealed a clear temporal transition from an initially weak and poorly differentiated geometry to a progressively more organised representational structure. In

the earliest windows (0-120 ms), the embeddings remained highly compact, with durations tightly clustered and little systematic separation between neighbouring values, consistent with the relatively undifferentiated RDMs observed at the same timepoints. From around 160-200 ms onward, however, the representational space expanded markedly and began to show a clear ordering with duration: shorter intervals (e.g., 400-800 ms) tended to occupy one side of the space, whereas longer intervals (e.g., 1800-2200 ms) progressively separated toward the opposite side. This change was mirrored in the RDMs, which became increasingly banded, with lower dissimilarities concentrated near the diagonal and larger dissimilarities emerging for pairs farther apart in duration. Thus, by about 200 ms after offset, EEG activity no longer appeared to reflect only a weak or generic post-stimulus response, but rather a structured representation preserving relational information between durations. Importantly, however, this emerging organisation was not exhausted by a simple magnitude-like ordering, and the subsequent analyses suggest that additional structuring principles also contributed to the geometry observed in this time range.

Crucially, in the $\approx$ 160-240 ms window, the RDMs exhibited an additional regularity that was not captured by a simple distance-from-diagonal gradient: dissimilarities appeared to depend not only on the absolute difference between two durations, but also on whether those durations occupied a similar position relative to the nearest oddball anchor (i.e., 70 ms or 3400 ms). In other words, durations that were similarly 'regular' with respect to these anchors - that is, that had a comparable distance to the closest odd duration - tended to evoke similar multivariate EEG patterns. This observation is important because it suggests that the neural geometry was already reflecting more than a straightforward short-to-long ordering. Instead, the representation appeared sensitive to a second-order property of the duration set: the relational status of each duration within the broader temporal context defined by the oddball anchors.

From approximately 200 ms onward, the embeddings showed a visually periodic component superimposed on the global short-to-long ordering, suggesting that the representational geometry was not strictly one-dimensional. Although the overall ordering of durations remained broadly preserved, the trajectory linking successive durations repeatedly bent back and forth through the space, revealing recurrent structure beyond monotonic scaling. This pattern is compatible with a second, cyclic organising principle layered on top of

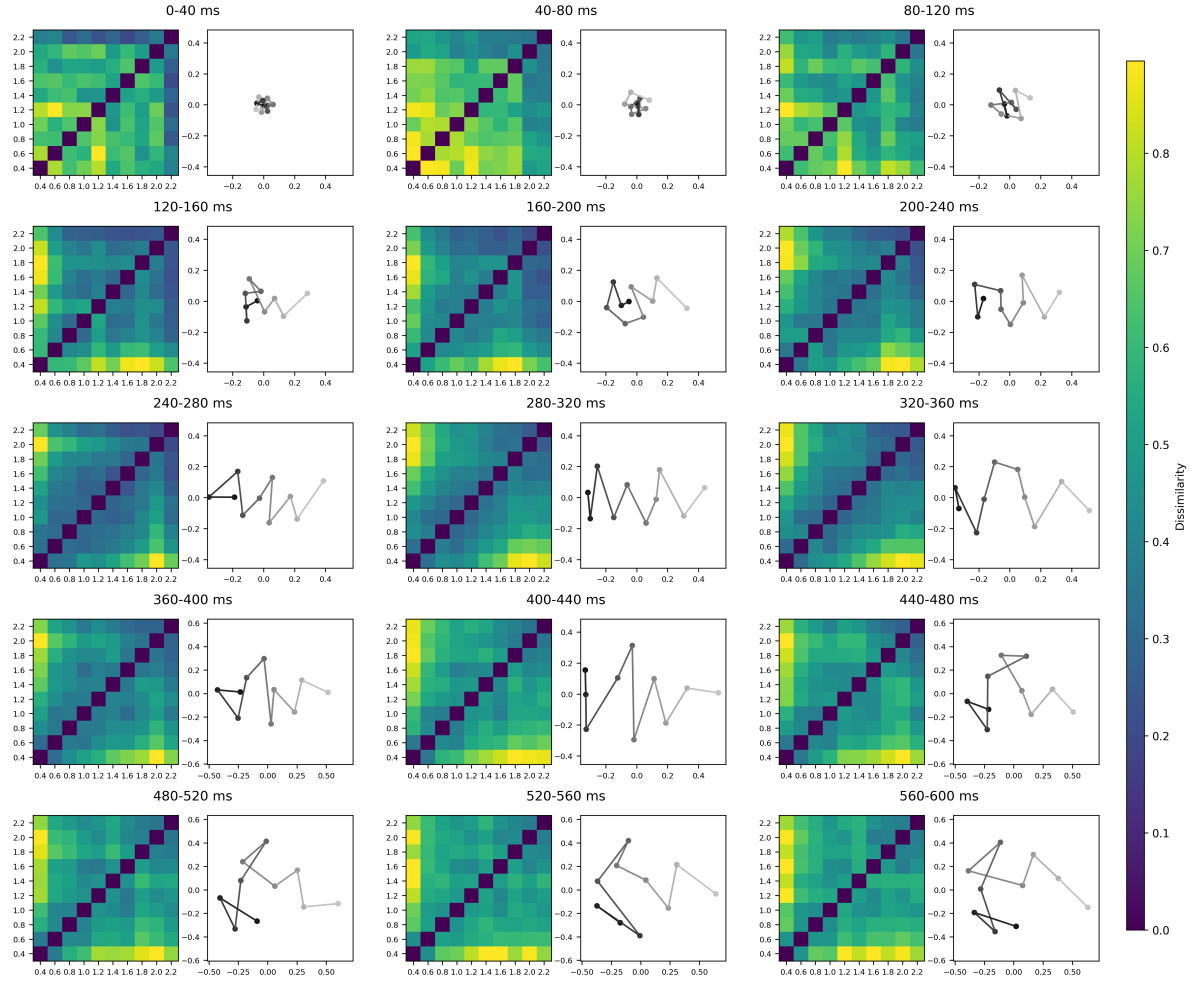

Figure 5. ***Dynamics of the neural geometry of duration space at stimulus offset***. *For each 40-ms time window from stimulus offset to 600 ms after offset, the left panel displays the group-average EEG representational dissimilarity matrix (RDM), in which each cell indicates the dissimilarity between the neural patterns evoked by a pair of stimulus durations. Lower values (blue) indicate more similar neural representations, whereas higher values (yellow) indicate more distinct representations. The right panel shows the corresponding 2D MDS solution for the same RDM, providing a geometric visualisation of the representational structure: durations plotted closer together were represented more similarly in the EEG signal, whereas durations plotted farther apart were represented more distinctly. Together, these panels illustrate how the geometry of duration space evolves over time following stimulus offset.*

the magnitude-like axis, such as an oscillatory or rhythmic component in similarity space.

Taken together, these observations suggest that the post-offset neural representation of duration is not adequately described as a simple linear magnitude code. Rather than collapsing onto a single magnitude axis, the neural representation of duration appeared to combine magnitude, anchor-relative, and periodic structure.

Representational similarity analysis

The MDS and RDM visualisations suggested that post-offset EEG activity progressively acquires a structured geometry, combining an overall magnitude-like ordering with additional relational and possibly periodic structure (Figure 5). We next asked whether

these qualitative impressions could be formalised using explicit theoretical models of duration representation. To do so, we used representational similarity analysis (RSA) and commonality analysis to quantify, at each timepoint, how much variance in the EEG RDMs could be explained by a set of candidate theoretical RDMs, both jointly and uniquely.

Figure 6 shows the results of these analyses. We first asked whether the emerging post-offset neural geometry was sufficiently structured to be captured by formal representational models at all. Figure 6A shows that the variance explained by the theoretical models increased sharply from approximately 100 ms after duration offset. The full model (dotted black line) provided a ceiling estimate of performance, accounting for approximately 40-50% of the total variance in the EEG RDMs, with peaks around 150 and 300 ms after offset. This indicates that the post-offset neural response was not only visually structured, but also organised enough to be captured to a great extent by a principled model space.

Having established that several models explained the neural data, we next asked whether they did so because they tracked the same structure as the behavioural similarity, or because they captured additional properties of the neural representation. The upcoming commonality analyses clarify this point. The variance shared with the Similarity model (Figure 6B) increased markedly after 100 ms and peaked around 300 ms. This was especially true for the best-performing structured models, for which a substantial part of their performance reflected representational structures also found in behavioural similarity judgements. This convergence is important because it links the post-offset neural geometry to the psychological geometry we characterised earlier. The two distinct levels of analysis (behaviour and EEG) recover a common representational organisation of duration.

Finally, we asked whether any model retained explanatory power beyond what could already be accounted for by behavioural similarity alone. Figure 6C shows that two models retained substantial *unique* explanatory power beyond Similarity: the Log model showed the most pronounced transient boost around 150–200 ms, together with a later rise toward the end of the analysis window. Additionally, the Regularness model explained unique variance during the early post-offset period. These results suggest that the neural representation is not exhausted by the behavioural similarity structure alone. Rather, shortly after duration offset, the EEG signal appears to express additional representational principles; most notably logarithmic and anchor-relative regularity structure; that are only partially reflected in

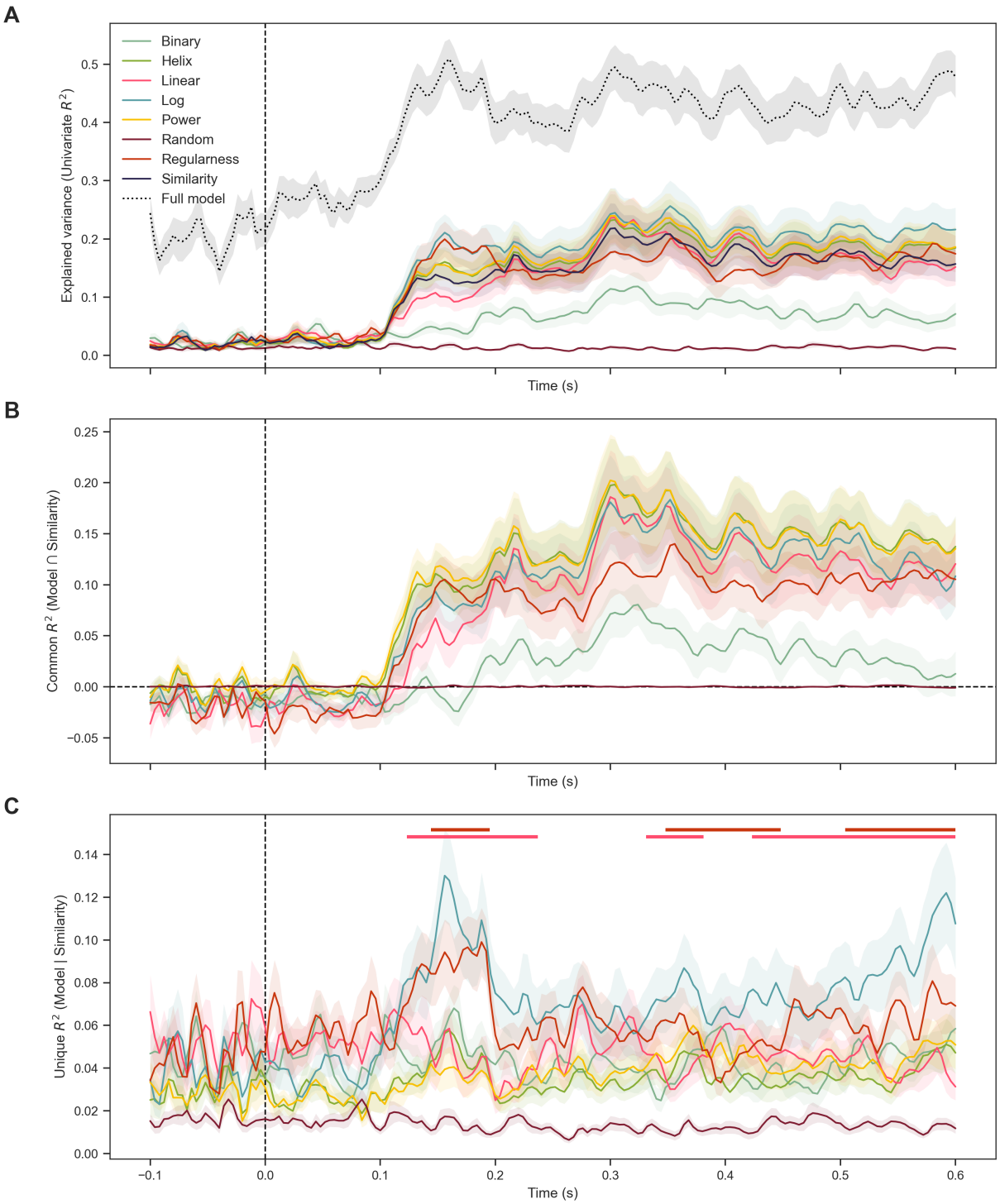

Figure 6. ***Group-level average EEG RSA and commonality results (+/- 1 SEM). A.*** *Explained variance for each predictor (as well as the full model).* ***B.*** *Explained variance between each model, the EEG RDM, and the behavioural similarity RDM.* ***C.*** *Unique variance explained by each model beyond the behavioural similarity RDM. The brown horizontal bar indicates the timesteps where the Log model explained more variance than the Regularness model, whereas the pink horizontal bar indicates the timesteps where the Log model explained more variance than the Linear model (model-based posterior odds above 20).*

explicit similarity judgements.

Together, these results suggest a constructive sequence in the emergence of post-offset duration representations: first, time-resolved neural responses become sufficiently structured

to be captured by formal models shortly after duration offset; second, a substantial part of this structure converges with the behavioural similarity geometry, especially around 300 ms; and third, some models; particularly Log and Regularness; capture additional neural variance around 150–200 ms that is not reducible to similarity judgements alone. Taken together, these findings indicate that the neural geometry of duration is both behaviourally grounded and richer than behavioural reports alone reveal.

Linking duration representations to neural dynamics

Task-related EEG correlates of duration representations

Having shown that duration is represented in the geometry of multivariate EEG patterns, we next asked whether this structure could also be detected in a simpler and classical electrophysiological signature of timing. We asked whether the post-offset P2 component (Baykan et al., 2023; Damsma et al., 2021; Kononowicz & Van Rijn, 2014; Ng et al., 2011; Ofir & Landau, 2022) varied with duration in a way that recapitulated the magnitude-like and potentially non-monotonic structure revealed by the representational analyses. To address this, we quantified the relation between objective duration and the P2 amplitude and latency.

Figure 7A shows the group-level average P2 amplitude and P2 latency. The amplitude of P2 was found to grow monotonically with objective duration. The amplitude-duration relationship was reliably monotonic ($\rho = 0.239$, $t(32) = 3.160, p = 0.0017$), consistent with a progressive increase of P2 amplitude with longer intervals. In contrast, the latency of P2 exhibited a weaker and more heterogeneous association with duration. Although latencies tended to increase with duration in the group average, the Spearman's correlation coefficient was smaller and did not reach significance ($\rho = 0.102$, $t(32) = 1.470$, $p = 0.0757$), suggesting that latency is not well captured by a simple monotonic trend and may instead reflect non-monotonic structure. Visual inspection of Figure 7 reveals local deviations from monotonicity around intermediate durations (1300 ms) and near the extreme durations. This pattern is reminiscent of the MDS pattern observed in the EEG RDMs (Figure 5) as well as in the behavioural data (Figure 2).

We found no significant correlations between participant-level mean P2 amplitude or latency, or oscillatory power at duration offset, and the parameter values of either the Helix or Power models.

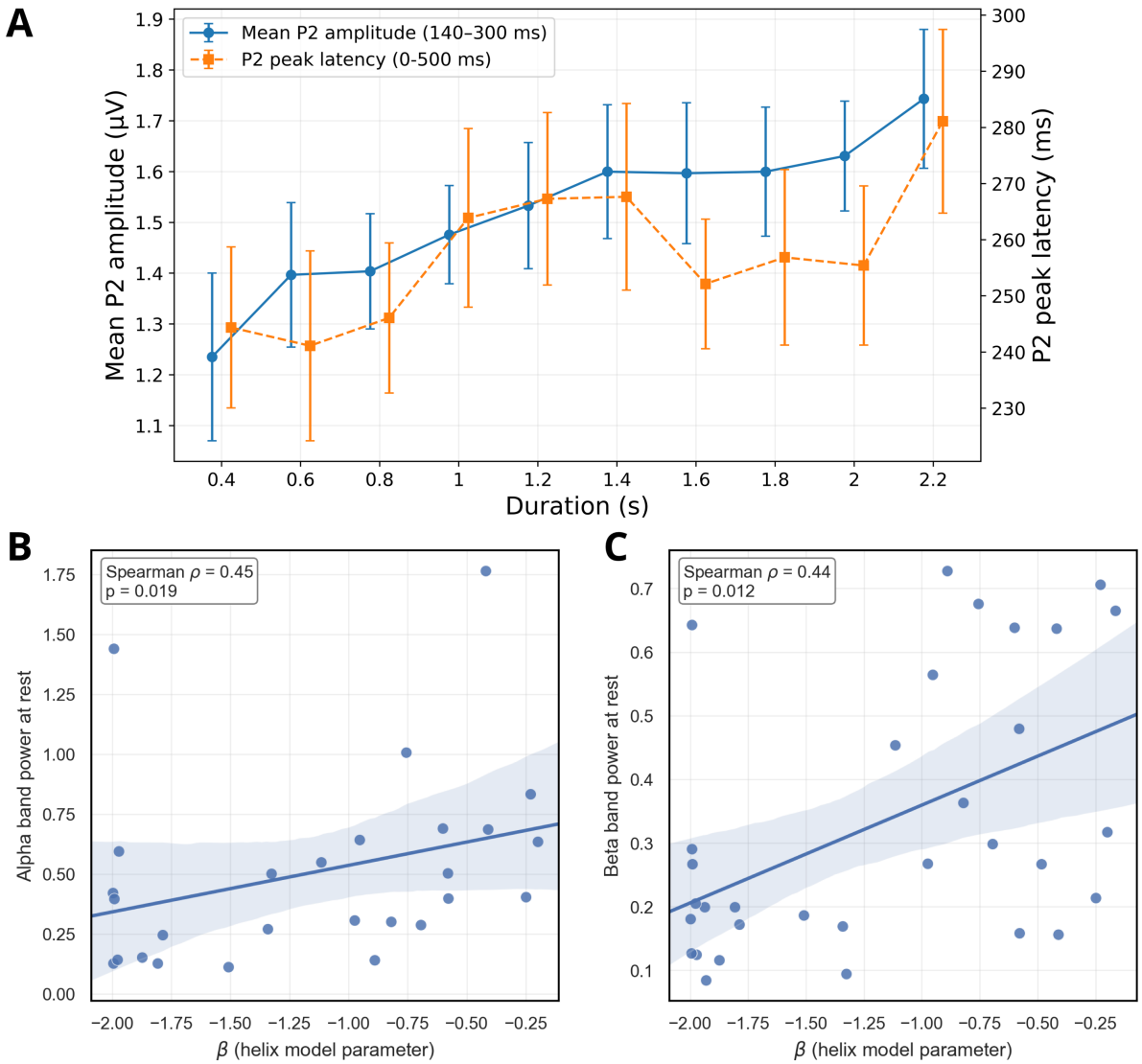

Figure 7. ***A.*** *Average P2 amplitude in the [140-300 ms] post-offset interval (blue, left y-axis) and P2 peak latency (orange curve, right y-axis). Dots represent the group-level mean and intervals represent the mean +/- 1 SEM.* ***B.*** *Relation between the participant-level estimated values of the β helix's parameter and the power in the alpha frequency band at rest.* ***C:*** *Relation between the participant-level estimated values of the β helix's parameter and the power in the beta frequency band at rest.*

Endogenous oscillatory correlates of duration representations

We next asked whether the geometry of duration space was related to more stable, endogenous properties of the individual's brain. To address this question, we tested whether inter-individual variation in the fitted parameters of the representational models was associated with resting-state oscillatory power, reasoning that intrinsic alpha and beta activity, both known for their implications in timing (Azizi et al., 2023; Bordas & Van Wassenhove, 2026; Kononowicz & Rijn, 2015; Kulashekhar et al., 2016; Mioni et al., 2020), might constrain how duration space is organised across participants (Figure 7B-C).

Figure 7 shows a positive correlation between the β helix parameter (governing

exponential growth of the radius, cf. Appendix A) and both the alpha (Figure 7B, Spearman's $\rho = 0.45,\ p = 0.019$) and beta (Figure 7C, Spearman's $\rho = 0.44,\ p = 0.012$) power at rest. This suggests that participants with stronger alpha and beta power also had smaller (closer to 0) helix β parameter, indicating a slower exponential growth of the helix's radius according to objective duration. In other words, participants with stronger alpha/beta power at rest had more spring-like helical structures, whereas participants with weaker alpha/beta power at rest had more conical helical structures, suggesting a stronger compression of larger durations. We found no other significant correlation between the Helix or Power model parameters and the endogenous oscillatory components we investigated.

Discussion

Duration is often treated as if it were represented along a single mental line running from short to long. The present results suggest a richer picture. Behavioural similarity judgements revealed a duration space structured not only by monotonic magnitude, but also by contextual position within the stimulus set and by a recurrent component not captured by standard scaling models. Time-resolved EEG analyses further showed that this structure emerges progressively after duration offset, with an early stage dominated by compressed and task-relevant coding and a later stage that more closely resembles behavioural similarity. These findings argue for a multidimensional and dynamic account of duration representation.

A 3D psychological geometry of duration space

The behavioural results provide the clearest evidence against a strictly one-dimensional account. First, as expected, durations were organised monotonically, with nearby durations judged as more similar than distant durations. This first dimension is consistent with a substantial literature suggesting that durations may be encoded monotonically, in a manner broadly analogous to other quantities. In the behavioural literature, this idea is often expressed through the notion of a mental timeline, according to which durations, like numbers, may be arranged along an ordered spatial axis, often from left to right (e.g., Bender & Beller, 2014; Bonato et al., 2012; Vallesi et al., 2008; Vicario et al., 2008). This proposal is supported by spatio-temporal congruency effects, whereby responses tend to be facilitated when short intervals or past-related concepts are mapped to the left side of space and long intervals or future-related concepts to the right (e.g., Casasanto & Bottini, 2010; Grasso et al., 2021, 2022a, 2022b; Vicario et al., 2008). More generally, interactions

between spatial and temporal dimensions are consistent with magnitude-based accounts such as A Theory of Magnitude (ATOM), which posits partially overlapping neural resources for processing time, space, and number (e.g., Bueti & Walsh, 2009; Walsh, 2003). Converging neuroimaging evidence has identified neuronal populations tuned to duration in cortical areas implicated timing and magnitude processing, including orderly topographic organisation of preferred durations in the supplementary motor area, described as chronomaps (Protopapa et al., 2018). Recent high-field fMRI work further suggests that duration coding follows a gradient from spatially dependent, monotonic encoding in early visual cortex to more abstract and spatially invariant coding in higher-level areas, culminating in the intraparietal cortex where spatial and temporal representations are closely intertwined (Centanino et al., 2024). Together, these findings support the idea that one major component of duration representation is a monotonic magnitude dimension.

However, the behavioural space also contained a second dimension reflecting eccentricity relative to the centre of the stimulus range, with a minimum close to the geometric mean of the duration set. This pattern is consistent with the long-standing observation that duration judgements are context sensitive and gravitate toward the central tendency of the experienced distribution (e.g., Karl von Vierordt, 1868; Shi & Burr, 2016; Shi et al., 2013). This pattern indicates that durations are not represented solely as absolute magnitudes, but relationally, with respect to the distribution in which they are embedded. Bayesian accounts formalise this by treating duration judgements as the combination of noisy sensory evidence with a learned prior over the stimulus distribution, naturally producing attraction toward the mean (Jazayeri & Shadlen, 2010; Petzschner et al., 2015; Zhu et al., 2021). Related modelling work further suggests that these effects are amplified when stimuli are randomised, or thought to be randomised (Glasauer & Shi, 2021, 2022; Nalborczyk, 2023). In geometric terms, this implies that the structure of duration space reflects the position of each duration relative to the central tendency of the set, rather than the magnitude ordering only.

A third feature of the behavioural duration space was a periodic-like component superimposed on the global duration ordering. This component is the most novel and also the most tentative aspect of the present findings. Importantly, we do not interpret it as evidence that duration is intrinsically ‘cyclic’ in the same strong sense as pitch chroma. Unlike tones separated by an octave, which are perceived as highly similar despite differing in pitch height,

durations that are far apart are clearly not experienced as equivalent or near-equivalent simply because they align at a similar 'phase' of the fitted helix. Rather, the periodic component we observe should be understood as a weaker, secondary modulation of similarity relations layered onto the dominant monotonic organisation of duration. In other words, it indicates that pairwise duration similarity contains recurrent structure not captured by magnitude scaling or contextual compression alone. In that sense, the generalised helix should be understood as a parsimonious geometric model of the data: it provides a compact way of combining monotonic progression with recurrent variation in a single latent trajectory. Its good behavioural fit, preserved under cross-validation, suggests that this geometry captures genuine structure in participants' judgements rather than merely overfitting idiosyncratic patterns. At the same time, the competitive performance of the Power model indicates that some aspects of the data can also be captured by monotonic nonlinearity alone. The main contribution of the helix is therefore not to replace all alternative models, but to make explicit that duration similarity may contain a recurrent component in addition to compression and ordering.

A dynamic neuronal geometry of duration space

The EEG results further suggest that this representational geometry is assembled over time following duration offset. Shortly after offset, neural dissimilarity structure was best captured by logarithmic and regularness-based models, peaking around 150 ms. This early stage is compatible with a compressed coding of elapsed duration and with the extraction of task-relevant information about how each standard duration relates to the oddball anchors. By contrast, around 300 ms after offset, the neural RDMs became more strongly aligned with behavioural similarity and with the broader family of structured models, including the Linear, Power, and Helix models. This temporal sequence suggests that post-offset activity does not simply reflect a static readout of elapsed time, but a transformation in representational format: from an early stage dominated by compressed and task-contingent coding to a later, more stable geometry resembling the structure expressed in explicit similarity judgements. On this view, behavioural similarity may reflect a relatively late representational format that integrates multiple constraints rather than a direct readout of the earliest duration code.

These findings have several implications for theories of timing. First, they are broadly compatible with magnitude-based accounts in showing that duration is organised monotonically, both behaviourally and neurally (e.g., Bonato et al., 2012; Vallesi et al., 2008;

Vicario et al., 2008). Second, they extend scalar and psychophysical accounts (Gallistel & Gibbon, 2000; Gibbon, 1977) by suggesting that compression is not merely a property of response variability, but is visible directly in the representational geometry itself. Third, they indicate that contextual structure, here expressed as distance to the geometric mean of the stimulus set, is not a secondary bias layered onto an otherwise metric representation, but may be one of the dimensions along which durations are encoded. This view is compatible with previous intracranial work in non-human primates showing that temporal context and prior expectations do not merely bias responses downstream, but reshape the geometry of population-level activity in frontal cortex during interval timing (Meirhaeghe et al., 2021; Sohn et al., 2019). Finally, the periodic component raises the possibility that endogenous neural dynamics contribute to the geometry of duration space (as previously suggested by Bailly et al., 2011). The positive association between resting alpha/beta power and the fitted helix β parameter provides convergent, though indirect, support for the idea that stable oscillatory properties of the brain may shape how durations are represented (e.g., timing precision Grabot et al., 2019). One possible interpretation is that the periodic component reflects a trace of recurrent sampling mechanisms, broadly consistent with proposals that oscillatory dynamics can provide temporal coordinates for interval timing (e.g., Gu et al., 2015; Pöppel, 1997; Van Wassenhove, 2016). However, the present data do not establish the mechanism underlying this component, and future work will be needed to determine whether it is genuinely oscillatory in origin, whether it depends on the specific range and spacing of the duration set, or whether it reflects a more general form of relational coding.

More generally, the present findings fit with a broader shift from axis-based to manifold-based accounts of neural representation (e.g., Jazayeri & Ostojic, 2021; Perich et al., 2025). In several domains, cognitive and perceptual variables are now understood as being encoded on low-dimensional manifolds embedded in higher-dimensional population activity, rather than along isolated scalar dimensions. In spatial cognition, for example, neural population activity has been shown to exhibit structured geometries including ring-like and toroidal manifolds, providing concrete examples of how continuous variables can be represented through recurrent low-dimensional organisation (e.g., Gardner et al., 2022; Russo et al., 2020). Our results suggest that duration may likewise be represented in a geometry that combines monotonic progression with recurrent structure. At a more conceptual level, the

cone-like expansion of the fitted generalised helix also resonates with broader attempts to think about temporality geometrically, including Bergson's cone model of memory (Bergson, 1896). These parallels remain heuristic rather than mechanistic, but they underscore a common point: once time is approached as a representational geometry, richer topologies than a simple line become both plausible and theoretically productive.

Several limitations should be acknowledged. First, the representational geometry was inferred from a specific set of auditory durations spanning 400 to 2200 ms in regular steps, so it remains unclear how far the recovered structure generalises across sensory modalities, temporal scales, and non-uniform sampling schemes. Second, behavioural similarity judgements provide a powerful window onto representational structure, but they may also reflect decision strategies that are specific to the explicit comparison tasks. Third, the EEG analyses provide fine temporal resolution but limited spatial precision, preventing strong anatomical claims about where these geometries are implemented. Finally, the correlations with endogenous brain rhythms are correlational and therefore do not establish a causal contribution of endogenous rhythms to the geometry of duration space.

Despite these limitations, the present findings provide a first step toward a geometric account of duration representation. Rather than supporting the idea of a single, one-dimensional, mental timeline, our results suggest that durations are organised in a richer representational space, structured behaviourally by monotonic, contextual, and periodic-like components, and expressed neurally through successive representational stages. More broadly, these results suggest that durations may be organised in a structured psychological space analogous, in principle, to perceptual spaces described in other domains. Characterising that space more fully may help bridge classical psychophysics, neural dynamics, and representational geometry, and provide a new framework for understanding how the mind and brain represent durations.

Data availability

All anonymised behavioural data and EEG epochs are freely available via the Open Science Framework: https://osf.io/vhcek/.

Code availability

All experimental material and analysis scripts are freely available via the Open Science Framework: https://osf.io/vhcek/.

Author contributions

Conceptualisation: CG, LN, VvW. Methodology: CG, LN, VvW. Software: CG, LN. Validation: VvW. Formal analysis: CG, LN. Investigation: CG, LN, VvW. Resources: VvW. Data curation: CG, LN. Writing - original draft: CG, LN. Writing - review and editing: CG, LN, VvW. Visualisation: CG, LN. Supervision: VvW. Project administration: VvW. Funding acquisition: VvW.

Competing interests

The authors declare no competing interests.

References

Azizi, L., Polti, I., & Van Wassenhove, V. (2023). Spontaneous alpha brain dynamics track the episodic "when". *The Journal of Neuroscience*, *43*(43), 7186–7197. https://doi.org/10.1523/JNEUROSCI.0816-23.2023

Bailly, F., Longo, G., & Montevil, M. (2011). A 2-dimensional geometry for biological time. *Progress in Biophysics and Molecular Biology*, *106*(3), 474–484. https://doi.org/10.1016/j.pbiomolbio.2011.02.001

Baykan, C., Zhu, X., Zinchenko, A., Müller, H. J., & Shi, Z. (2023). Electrophysiological signatures of temporal context in the bisection task. *Experimental Brain Research*, *241*(8), 2081–2096. https://doi.org/10.1007/s00221-023-06670-1

Bender, A., & Beller, S. (2014). Mapping spatial frames of reference onto time: A review of theoretical accounts and empirical findings. *Cognition*, *132*(3), 342–382. https://doi.org/10.1016/j.cognition.2014.03.016

Bergson, H. (1896). *Matière et mémoire: Essai sur la relation du corps à l'esprit*. Félix Alcan.

Bonato, M., Zorzi, M., & Umiltà, C. (2012). When time is space: Evidence for a mental time line. *Neuroscience & Biobehavioral Reviews*, *36*(10), 2257–2273. https://doi.org/10.1016/j.neubiorev.2012.08.007

Bordas, R., & Van Wassenhove, V. (2026). Spontaneous oscillatory activity in episodic timing: An EEG replication study and its limitations. *eneuro*, *13*(1), ENEURO.0332–25.2025. https://doi.org/10.1523/ENEURO.0332-25.2025

Bueti, D., & Walsh, V. (2009). The parietal cortex and the representation of time, space, number and other magnitudes. *Philosophical Transactions of the Royal Society B: Biological Sciences*, *364*(1525), 1831–1840. https://doi.org/10.1098/rstb.2009.0028

Buonomano, D. V., Buzsáki, G., Davachi, L., & Nobre, A. C. (2023). Time for memories. *The Journal of Neuroscience*, *43*(45), 7565–7574. https://doi.org/10.1523/JNEUROSCI.1430-23.2023

Bürkner, P.-C. (2017). **brms** : An *R* package for bayesian multilevel models using *Stan*. *Journal of Statistical Software*, *80*(1). https://doi.org/10.18637/jss.v080.i01

Bürkner, P.-C. (2018). Advanced bayesian multilevel modeling with the r package brms. *The R Journal*, *10*(1), 395–411. Retrieved June 11, 2019, from https://journal.r-project.org/archive/2018/RJ-2018-017/index.html

Buzsáki, G. (2026). Time, space, memory and brain–body rhythms. *Nature Reviews Neuroscience*, *27*(1), 61–78. https://doi.org/10.1038/s41583-025-00987-2

Casasanto, D., & Bottini, R. (2010). Can Mirror-Reading Reverse the Flow of Time? [Series Title: Lecture Notes in Computer Science]. In D. Hutchison, T. Kanade, J. Kittler, J. M. Kleinberg, F. Mattern, J. C. Mitchell, M. Naor, O. Nierstrasz, C. Pandu Rangan, B. Steffen, M. Sudan, D. Terzopoulos, D. Tygar, M. Y. Vardi, G. Weikum, C. Hölscher, T. F. Shipley, M. Olivetti Belardinelli, J. A. Bateman, & N. S. Newcombe (Eds.), *Spatial Cognition VII* (pp. 335–345, Vol. 6222). Springer Berlin Heidelberg. https://doi.org/10.1007/978-3-642-14749-4_28

Centanino, V., Fortunato, G., & Bueti, D. (2024). The neural link between stimulus duration and spatial location in the human visual hierarchy. *Nature Communications*, *15*(1), 10720. https://doi.org/10.1038/s41467-024-54336-5

Chang, A., Poeppel, D., & Teng, X. (2025). Temporally dissociable neural representations of pitch height and chroma. *The Journal of Neuroscience*, *45*(8), e1567242024. https://doi.org/10.1523/JNEUROSCI.1567-24.2024

Chung, S., & Abbott, L. (2021). Neural population geometry: An approach for understanding biological and artificial neural networks. *Current Opinion in Neurobiology*, *70*, 137–144. https://doi.org/10.1016/j.conb.2021.10.010

Cichy, R. M., & Oliva, A. (2020). A m/EEG-fMRI fusion primer: Resolving human brain responses in space and time. *Neuron*, *107*(5), 772–781. https://doi.org/10.1016/j.neuron.2020.07.001

Cohen, M. X. (2014, January). *Analyzing Neural Time Series Data: Theory and Practice*. The MIT Press. https://doi.org/10.7551/mitpress/9609.001.0001

Dai, H., & Micheyl, C. (2010). On the choice of adequate randomization ranges for limiting the use of unwanted cues in same-different, dual-pair, and oddity tasks. *Attention, Perception, & Psychophysics*, *72*(2), 538–547. https://doi.org/10.3758/APP.72.2.538

Damsma, A., Schlichting, N., & Van Rijn, H. (2021). Temporal context actively shapes EEG signatures of time perception. *The Journal of Neuroscience*, *41*(20), 4514–4523. https://doi.org/10.1523/JNEUROSCI.0628-20.2021

David, O., Kilner, J. M., & Friston, K. J. (2006). Mechanisms of evoked and induced responses in MEG/EEG. *NeuroImage*, *31*(4), 1580–1591. https://doi.org/10.1016/j.neuroimage.2006.02.034

Donoghue, T., Haller, M., Peterson, E. J., Varma, P., Sebastian, P., Gao, R., Noto, T., Lara, A. H., Wallis, J. D., Knight, R. T., Shestyuk, A., & Voytek, B. (2020). Parameterizing neural power spectra into periodic and aperiodic components. *Nature Neuroscience*, *23*(12), 1655–1665. https://doi.org/10.1038/s41593-020-00744-x

Fournel, A., Ferdenzi, C., Sezille, C., Rouby, C., & Bensafi, M. (2016). Multidimensional representation of odors in the human olfactory cortex: Odor Neural Spaces. *Human Brain Mapping*, *37*(6), 2161–2172. https://doi.org/10.1002/hbm.23164

Gallistel, C. R. (1990). *The organization of learning*. MIT Press.

Gallistel, C. R., & Gibbon, J. (2000). Time, rate, and conditioning. *Psychological Review*, *107*(2), 289–344. https://doi.org/10.1037/0033-295X.107.2.289

Gardner, R. J., Hermansen, E., Pachitariu, M., Burak, Y., Baas, N. A., Dunn, B. A., Moser, M.-B., & Moser, E. I. (2022). Toroidal topology of population activity in grid cells. *Nature*, *602*(7895), 123–128. https://doi.org/10.1038/s41586-021-04268-7

Gibbon, J. (1977). Scalar expectancy theory and Weber's law in animal timing. *Psychological Review*, *84*(3), 279–325. https://doi.org/10.1037/0033-295X.84.3.279

Glasauer, S., & Shi, Z. (2021). The origin of vierordt's law: The experimental protocol matters. *PsyCh Journal*, *10*(5), 732–741. https://doi.org/10.1002/pchj.464

Glasauer, S., & Shi, Z. (2022). Individual beliefs about temporal continuity explain variation of perceptual biases. *Scientific Reports*, *12*(1), 10746. https://doi.org/10.1038/s41598-022-14939-8

Gower, J. C. (1975). Generalized procrustes analysis. *Psychometrika*, *40*(1), 33–51. https://doi.org/10.1007/BF02291478

Grabot, L., Kononowicz, T. W., Dupré La Tour, T., Gramfort, A., Doyère, V., & Van Wassenhove, V. (2019). The Strength of Alpha–Beta Oscillatory Coupling Predicts Motor Timing Precision. *The Journal of Neuroscience*, *39*(17), 3277–3291. https://doi.org/10.1523/JNEUROSCI.2473-18.2018

Gramfort, A. (2013). MEG and EEG data analysis with MNE-python. *Frontiers in Neuroscience*, *7*. https://doi.org/10.3389/fnins.2013.00267

Grasso, C. L., Ziegler, J. C., Coull, J. T., & Montant, M. (2022a). Space–Time Congruency Effects Using Eye Movements During Processing of Past- and Future-Related Words. *Experimental Psychology*, *69*(4), 210–217. https://doi.org/10.1027/1618-3169/a000559

Grasso, C. L., Ziegler, J. C., Coull, J. T., & Montant, M. (2022b). Embodied time: Effect of reading expertise on the spatial representation of past and future (L. Barca, Ed.). *PLOS ONE*, *17*(10), e0276273. https://doi.org/10.1371/journal.pone.0276273

Grasso, C. L., Ziegler, J. C., Mirault, J., Coull, J. T., & Montant, M. (2021). As time goes by: Space-time compatibility effects in word recognition. *Journal of Experimental Psychology: Learning, Memory, and Cognition*. https://doi.org/10.1037/xlm0001007

Gu, B.-M., Van Rijn, H., & Meck, W. H. (2015). Oscillatory multiplexing of neural population codes for interval timing and working memory. *Neuroscience & Biobehavioral Reviews*, *48*, 160–185. https://doi.org/10.1016/j.neubiorev.2014.10.008

Hebart, M. N., Bankson, B. B., Harel, A., Baker, C. I., & Cichy, R. M. (2018). The representational dynamics of task and object processing in humans. *eLife*, *7*, e32816. https://doi.org/10.7554/eLife.32816

Jazayeri, M., & Ostojic, S. (2021). Interpreting neural computations by examining intrinsic and embedding dimensionality of neural activity. *Current Opinion in Neurobiology*, *70*, 113–120. https://doi.org/10.1016/j.conb.2021.08.002

Jazayeri, M., & Shadlen, M. N. (2010). Temporal context calibrates interval timing. *Nature Neuroscience*, *13*(8), 1020–1026. https://doi.org/10.1038/nn.2590

Karl von Vierordt. (1868). *Der zeitsinn nach versuchen*. H. Laupp. Retrieved September 28, 2022, from http://archive.org/details/derzeitsinnnach00viergoog

Kawakita, G., Zeleznikow-Johnston, A., Takeda, K., Tsuchiya, N., & Oizumi, M. (2025). Is my "red" your "red"?: Evaluating structural correspondences between color similarity judgments using unsupervised alignment. *iScience*, *28*(3), 112029. https://doi.org/10.1016/j.isci.2025.112029

Kawakita, G., Zeleznikow-Johnston, A., Tsuchiya, N., & Oizumi, M. (2024). Gromov–wasserstein unsupervised alignment reveals structural correspondences between the color similarity structures of humans and large language models. *Scientific Reports*, *14*(1), 15917. https://doi.org/10.1038/s41598-024-65604-1

Kononowicz, T. W., & Rijn, H. V. (2015). Single trial beta oscillations index time estimation. *Neuropsychologia*, *75*, 381–389. https://doi.org/10.1016/j.neuropsychologia.2015.06.014

Kononowicz, T. W., & Van Rijn, H. (2014). Decoupling interval timing and climbing neural activity: A dissociation between CNV and n1p2 amplitudes. *The Journal of Neuroscience*, *34*(8), 2931–2939. https://doi.org/10.1523/JNEUROSCI.2523-13.2014

Kriegeskorte, N., & Kievit, R. A. (2013). Representational geometry: Integrating cognition, computation, and the brain. *Trends in Cognitive Sciences*, *17*(8), 401–412. https://doi.org/10.1016/j.tics.2013.06.007

Kriegeskorte, N., Mur, M., Ruff, D. A., Kiani, R., Bodurka, J., Esteky, H., Tanaka, K., & Bandettini, P. A. (2008). Matching Categorical Object Representations in Inferior Temporal Cortex of Man and Monkey. *Neuron*, *60*(6), 1126–1141. https://doi.org/10.1016/j.neuron.2008.10.043

Kruskal, J. B. (1964). Multidimensional scaling by optimizing goodness of fit to a nonmetric hypothesis. *Psychometrika*, *29*(1), 1–27. https://doi.org/10.1007/BF02289565

Kruskal, J. B., & Wish, M. (1978). *Multidimensional scaling*. SAGE Publications, Inc. https://doi.org/10.4135/9781412985130

Kulashekhar, S., Pekkola, J., Palva, J. M., & Palva, S. (2016). The role of cortical beta oscillations in time estimation. *Human Brain Mapping*, *37*(9), 3262–3281. https://doi.org/10.1002/hbm.23239

Kwok, S. C., Lapate, R. C., Sakon, J. J., Van Wassenhove, V., Xue, G., & Zheng, J. (2025). Neural representation of episodic time. *The Journal of Neuroscience*, *45*(46), e1397252025. https://doi.org/10.1523/JNEUROSCI.1397-25.2025

Ma, A. C., Cameron, A. D., & Wiener, M. (2024). Memorability shapes perceived time (and vice versa). *Nature Human Behaviour*, *8*(7), 1296–1308. https://doi.org/10.1038/s41562-024-01863-2

Marjieh, R., Griffiths, T. L., & Jacoby, N. (2023, June). Pitch is Not (Always) a Helix: Probing the Structure of Musical Pitch Across Tasks and Experience. https://doi.org/10.1101/2023.06.13.544763

Marjieh, R., Sucholutsky, I., Van Rijn, P., Jacoby, N., & Griffiths, T. L. (2024). Large language models predict human sensory judgments across six modalities. *Scientific Reports*, *14*(1), 21445. https://doi.org/10.1038/s41598-024-72071-1

Meirhaeghe, N., Sohn, H., & Jazayeri, M. (2021). A precise and adaptive neural mechanism for predictive temporal processing in the frontal cortex. *Neuron*, *109*(18), 2995–3011.e5. https://doi.org/10.1016/j.neuron.2021.08.025

Mioni, G., Shelp, A., Stanfield-Wiswell, C. T., Gladhill, K. A., Bader, F., & Wiener, M. (2020). Modulation of individual alpha frequency with tACS shifts time perception. *Cerebral Cortex Communications*, *1*(1), tgaa064. https://doi.org/10.1093/texcom/tgaa064

Nalborczyk, L. (2023). When randomization hurts. *Nature Reviews Psychology*, *2*(3), 131–131. https://doi.org/10.1038/s44159-023-00155-2

Nalborczyk, L., Batailler, C., Lœvenbruck, H., Vilain, A., & Bürkner, P.-C. (2019). An introduction to bayesian multilevel models using brms: A case study of gender effects on vowel variability in standard indonesian. *Journal of Speech Language and Hearing Research*, *62*(5), 1225–1242. https://doi.org/10.1044/2018_JSLHR-S-18-0006

Nalborczyk, L., & Bürkner, P. (2025, August 31). Precise temporal localisation of m/EEG effects with bayesian generalised additive multilevel models. https://doi.org/10.1101/2025.08.29.672336

Ng, K. K., Tobin, S., & Penney, T. B. (2011). Temporal accumulation and decision processes in the duration bisection task revealed by contingent negative variation. *Frontiers in Integrative Neuroscience*, *5*. https://doi.org/10.3389/fnint.2011.00077

Nieh, E. H., Schottdorf, M., Freeman, N. W., Low, R. J., Lewallen, S., Koay, S. A., Pinto, L., Gauthier, J. L., Brody, C. D., & Tank, D. W. (2021). Geometry of abstract learned knowledge in the hippocampus. *Nature*, *595*(7865), 80–84. https://doi.org/10.1038/s41586-021-03652-7

Ofir, N., & Landau, A. N. (2022). Neural signatures of evidence accumulation in temporal decisions. *Current Biology*, *32*(18), 4093–4100.e6. https://doi.org/10.1016/j.cub.2022.08.006

Paton, J. J., & Buonomano, D. V. (2018). The Neural Basis of Timing: Distributed Mechanisms for Diverse Functions. *Neuron*, *98*(4), 687–705. https://doi.org/10.1016/j.neuron.2018.03.045

Peirce, J., Gray, J. R., Simpson, S., MacAskill, M., Höchenberger, R., Sogo, H., Kastman, E., & Lindeløv, J. K. (2019). PsychoPy2: Experiments in behavior made easy. *Behavior Research Methods*, *51*(1), 195–203. https://doi.org/10.3758/s13428-018-01193-y

Perich, M. G., Narain, D., & Gallego, J. A. (2025). A neural manifold view of the brain. *Nature Neuroscience*, *28*(8), 1582–1597. https://doi.org/10.1038/s41593-025-02031-z

Petzschner, F. H., Glasauer, S., & Stephan, K. E. (2015). A Bayesian perspective on magnitude estimation. *Trends in Cognitive Sciences*, *19*(5), 285–293. https://doi.org/10.1016/j.tics.2015.03.002

Pöppel, E. (1997). A hierarchical model of temporal perception. *Trends in Cognitive Sciences*, *1*(2), 56–61. https://doi.org/10.1016/S1364-6613(97)01008-5

Protopapa, F., Hayashi, M. J., Kulashekhar, S., der Zwaag, W. v., Battistella, G., Murray, M. M., Kanai, R., & Bueti, D. (2018, August). *Chronotopic Maps in Human Medial Premotor Cortex* (preprint). Neuroscience. https://doi.org/10.1101/399857

Rattat, A.-C., & Droit-Volet, S. (2012). What is the best and easiest method of preventing counting in different temporal tasks? *Behavior Research Methods*, *44*(1), 67–80. https://doi.org/10.3758/s13428-011-0135-3

Rosenthal, I. A., Singh, S. R., Hermann, K. L., Pantazis, D., & Conway, B. R. (2021). Color Space Geometry Uncovered with Magnetoencephalography. *Current Biology*, *31*(3), 515–526.e5. https://doi.org/10.1016/j.cub.2020.10.062

Russo, A. A., Khajeh, R., Bittner, S. R., Perkins, S. M., Cunningham, J. P., Abbott, L., & Churchland, M. M. (2020). Neural trajectories in the supplementary motor area and motor cortex exhibit distinct geometries, compatible with different classes of computation. *Neuron*, *107*(4), 745–758.e6. https://doi.org/10.1016/j.neuron.2020.05.020

Seibold, D. R., & McPhee, R. D. (1979). Commonality analysis: A method for decomposing explained variance in multiple regression analyses. *Human Communication Research*, *5*(4), 355–365. https://doi.org/10.1111/j.1468-2958.1979.tb00649.x

Shepard, R. N. (1980). Multidimensional scaling, tree-fitting, and clustering. *Science*, *210*(4468), 390–398. https://doi.org/10.1126/science.210.4468.390

Shepard, R. N. (1982). Geometrical approximations to the structure of musical pitch. *Psychological Review*, *89*(4), 305–333. https://doi.org/10.1037/0033-295X.89.4.305

Shepard, R. N. (1987). Toward a Universal Law of Generalization for Psychological Science. *Science*, *237*(4820), 1317–1323. https://doi.org/10.1126/science.3629243

Shepard, R. N., & Chipman, S. (1970). Second-order isomorphism of internal representations: Shapes of states. *Cognitive Psychology*, *1*(1), 1–17. https://doi.org/10.1016/0010-0285(70)90002-2

Shepard, R. N., & Cooper, L. A. (1992). Representation of colors in the blind, color-blind, and normally sighted. *Psychological Science*, *3*(2), 97–104. Retrieved August 31, 2023, from https://www.jstor.org/stable/40062765

Shepard, R. N., Kilpatric, D. W., & Cunningham, J. P. (1975). The internal representation of numbers. *Cognitive Psychology*, *7*(1), 82–138. https://doi.org/10.1016/0010-0285(75)90006-7

Shi, Z., & Burr, D. (2016). Predictive coding of multisensory timing. *Current Opinion in Behavioral Sciences*, *8*, 200–206. https://doi.org/10.1016/j.cobeha.2016.02.014

Shi, Z., Church, R. M., & Meck, W. H. (2013). Bayesian optimization of time perception. *Trends in Cognitive Sciences*, *17*(11), 556–564. https://doi.org/10.1016/j.tics.2013.09.009

Sievers, B., Parkinson, C., Kohler, P. J., Hughes, J. M., Fogelson, S. V., & Wheatley, T. (2021). Visual and auditory brain areas share a representational structure that supports emotion perception. *Current Biology*, *31*(23), 5192–5203.e4. https://doi.org/10.1016/j.cub.2021.09.043

Smith, S., & Nichols, T. (2009). Threshold-free cluster enhancement: Addressing problems of smoothing, threshold dependence and localisation in cluster inference. *NeuroImage*, *44*(1), 83–98. https://doi.org/10.1016/j.neuroimage.2008.03.061

Sohn, H., Narain, D., Meirhaeghe, N., & Jazayeri, M. (2019). Bayesian computation through cortical latent dynamics. *Neuron*, *103*(5), 934–947.e5. https://doi.org/10.1016/j.neuron.2019.06.012

Stevens, S. S. (1957). On the psychophysical law. *Psychological Review*, *64*(3), 153–181. https://doi.org/10.1037/h0046162

Tamir, D. I., Thornton, M. A., Contreras, J. M., & Mitchell, J. P. (2016). Neural evidence that three dimensions organize mental state representation: Rationality, social impact, and valence. *Proceedings of the National Academy of Sciences*, *113*(1), 194–199. https://doi.org/10.1073/pnas.1511905112

961 Thornton, M. A., & Mitchell, J. P. (2018). Theories of Person Perception Predict Patterns of
962 Neural Activity During Mentalizing. *Cerebral Cortex*, *28*(10), 3505–3520.
963 https://doi.org/10.1093/cercor/bhx216
964 Torgerson, W. S. (1977). *Theory and methods of scaling* (16. Dr.). Wiley.
965 Tsao, A., Yousefzadeh, S. A., Meck, W. H., Moser, M.-B., & Moser, E. I. (2022). The neural
966 bases for timing of durations. *Nature Reviews Neuroscience*, *23*(11), 646–665.
967 https://doi.org/10.1038/s41583-022-00623-3
968 Ueda, K., & Ohgushi, K. (1987). Perceptual components of pitch: Spatial representation using
969 a multidimensional scaling technique. *The Journal of the Acoustical Society of*
970 *America*, *82*(4), 1193–1200. https://doi.org/10.1121/1.395255
971 Vallesi, A., Binns, M. A., & Shallice, T. (2008). An effect of spatial–temporal association of
972 response codes: Understanding the cognitive representations of time. *Cognition*,
973 *107*(2), 501–527. https://doi.org/10.1016/j.cognition.2007.10.011
974 Van Baar, J. M., Chang, L. J., & Sanfey, A. G. (2019). The computational and neural
975 substrates of moral strategies in social decision-making. *Nature Communications*,
976 *10*(1), 1483. https://doi.org/10.1038/s41467-019-09161-6
977 Van Vliet, M., Appelhoff, S., Shimizu, T., Eremin, E., Hultén, A., Zhao, Y., &
978 Höchenberger, R. (2025). MNE-RSA: Representational similarity analysis on EEG,
979 MEG and fMRI data. *Journal of Open Source Software*, *10*(116), 9148.
980 https://doi.org/10.21105/joss.09148
981 Van Wassenhove, V. (2016). Temporal cognition and neural oscillations. *Current Opinion in*
982 *Behavioral Sciences*, *8*, 124–130. https://doi.org/10.1016/j.cobeha.2016.02.012
983 van Wassenhove, V. (2009). Minding time in an amodal representational space. *Philosophical*
984 *Transactions of the Royal Society B: Biological Sciences*, *364*(1525), 1815–1830.
985 https://doi.org/10.1098/rstb.2009.0023
986 Vicario, C. M., Pecoraro, P., Turriziani, P., Koch, G., Caltagirone, C., & Oliveri, M. (2008).
987 Relativistic Compression and Expansion of Experiential Time in the Left and Right
988 Space (C. Miall, Ed.). *PLoS ONE*, *3*(3), e1716.
989 https://doi.org/10.1371/journal.pone.0001716

990 Walsh, V. (2003). A theory of magnitude: Common cortical metrics of time, space and
991 quantity. *Trends in Cognitive Sciences*, *7*(11), 483–488.
992 https://doi.org/10.1016/j.tics.2003.09.002
993 Zeleznikow-Johnston, A., Aizawa, Y., Yamada, M., & Tsuchiya, N. (2023). Are color
994 experiences the same across the visual field? *Journal of Cognitive Neuroscience*, *35*(4),
995 509–542. https://doi.org/10.1162/jocn_a_01962
996 Zhu, X., Baykan, C., Müller, H. J., & Shi, Z. (2021). Temporal bisection is influenced by
997 ensemble statistics of the stimulus set. *Attention, Perception, & Psychophysics*, *83*(3),
998 1201–1214. https://doi.org/10.3758/s13414-020-02202-z

Appendix A

Generalised helix model

In this embedding-based model, each duration d is mapped onto a point in a three-dimensional latent space lying on a parametrised helical trajectory. The geometry of the helix is defined by three components:

- **Radial growth:**

$$r(d) = r_0\, e^{\beta d},$$

  where β determines how the radius expands as a function of duration d.

- **Angular component:**

$$\theta(d) = \omega d,$$

  where ω sets the angular velocity (number of turns).

- **Vertical (z-axis) component:**

$$z(d) = p\, e^{\kappa d},$$

  where p is the pitch (vertical spacing between turns) and κ determines exponential expansion along the vertical axis.

Combining these components, each duration is embedded in $\mathbb{R}^3$ as:

$$\mathbf{x}(d) = \begin{pmatrix} r(d)\cos\theta(d) \\ r(d)\sin\theta(d) \\ z(d) \end{pmatrix}.$$

The predicted dissimilarity between two durations d_i and d_j is given by their Euclidean distance in this latent space:

$$\mathcal{M}_{\text{helix}}(d_i, d_j \mid \Theta) = \|\mathbf{x}(d_i) - \mathbf{x}(d_j)\|_2 = \sqrt{(x_i - x_j)^2 + (y_i - y_j)^2 + (z_i - z_j)^2},$$

where $\Theta_{\text{helix}} = \{r_0, \beta, p, \omega, \kappa\}$ denotes the set of helix parameters. In the present study, a subset of these parameters was held constant ($\{r_0 = 0.1, p = 1\}$), κ and β were further assumed to be equal, and the remaining *two free parameters* (i.e., β and ω) were optimised

separately for each participant by maximising the Spearman correlation between the model-predicted RDM and the empirical RDM. We provide a Shiny application allowing to interact with the parameters of this model and visualise its predictions: https://lnalborczyk.github.io/apps/helix.

Appendix B

Participant-level behavioural RDMs

Figure B1 shows the average symmetrised empirical RDM computed using the similarity judgements for each participant. As can been seen from this figure, participants showed a great amount of variability. Whereas all participants tended to show a clear diagonal pattern, and although these matrices contain the average of 2 order × 4 repetitions = 8 similarity ratings (for each pair of durations), participants varied in the precision of this pattern (i.e., dispersion around the diagonal), whether the subjective diagonal isochrony line coincided with the objective isochrony line (i.e., the matrix diagonal), or whether dispersion around the diagonal tended to increase (or to remain stable) with duration.

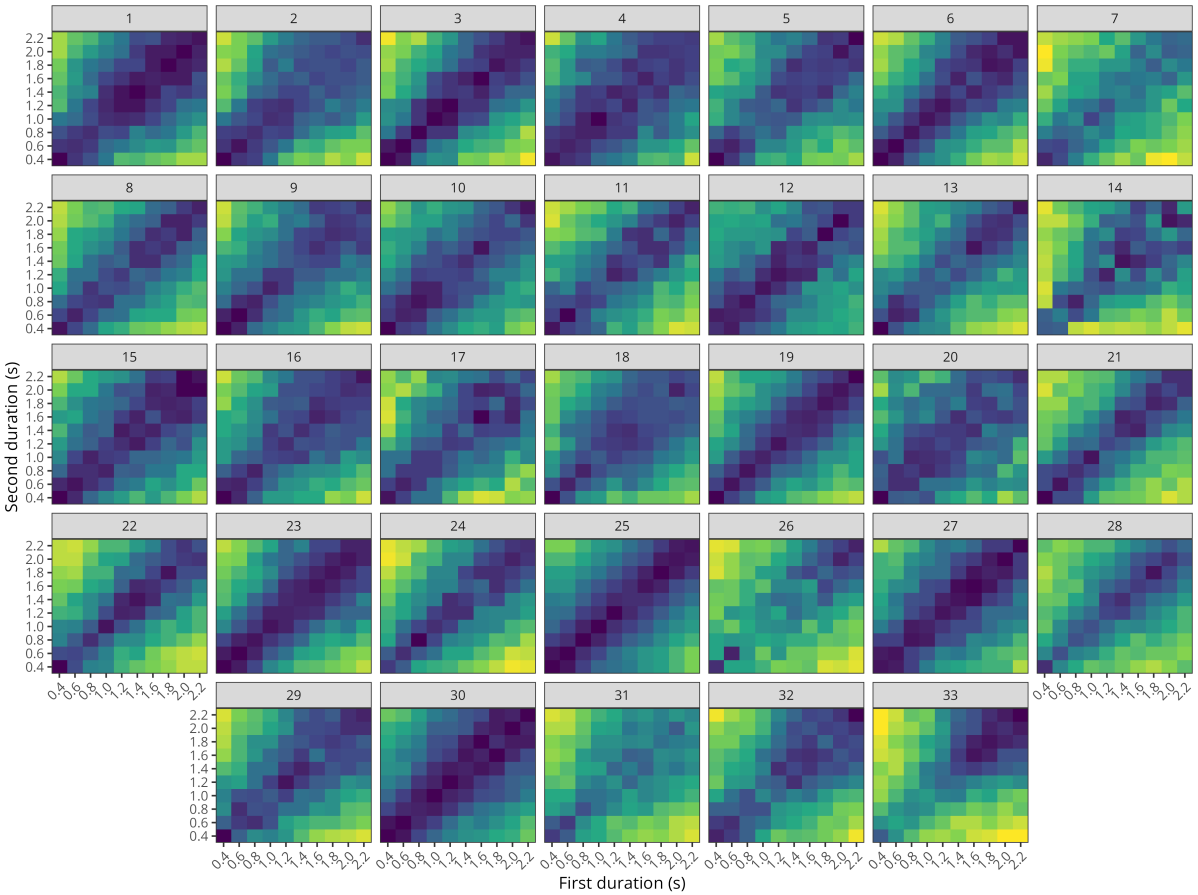

Figure B1. *Participant-level average symmetrised behavioural RDMs.*